Title

Calponin homology domain containing kinesin, KIS1, regulates chloroplast stromule formation and immunity

Journal

Science Advances, 9(43)

ISSN

2375-2548

Authors

Meier, Nathan D

Seward, Kody

Caplan, Jeffrey L

et al.

Publication Date

2023-10-27

DOI

10.1126/sciadv.adi7407

PLANT SCIENCES

Calponin homology domain containing kinesin, KIS1, regulates chloroplast stromule formation and immunity

Nathan D. Meier[1], Kody Seward[2,3]†, Jeffrey L. Caplan[2,3,4]*, Savithramma P. Dinesh-Kumar[1]*

Chloroplast morphology changes during immunity, giving rise to tubule-like structures known as stromules. Stromules extend along microtubules and anchor to actin filaments along nuclei to promote perinuclear chloroplast clustering. This facilitates the transport of defense molecules/proteins from chloroplasts to the nucleus. Evidence for a direct role for stromules in immunity is lacking since, currently, there are no known genes that regulate stromule biogenesis. We show that a calponin homology (CH) domain containing kinesin, KIS1 (kinesin required for inducing stromules 1), is required for stromule formation during TNL [TIR (Toll/Interleukin-1 receptor)-type nucleotide-binding leucine-rich repeat]-immune receptor-mediated immunity. Furthermore, KIS1 is required for TNL-mediated immunity to bacterial and viral pathogens. The microtubule-binding motor domain of KIS1 is required for stromule formation while the actin-binding, CH domain is required for perinuclear chloroplast clustering. We show that KIS1 functions through early immune signaling components, EDS1 and PAD4, with salicylic acid–induced stromules requiring KIS1. Thus, KIS1 represents a player in stromule biogenesis.

INTRODUCTION

Plants have evolved with a sophisticated immune system that can effectively defend against invading microbes. The primary immune response to pathogenic microbes is triggered by cell-surface localized pattern-recognition receptors (PRRs) (*1*). PRRs directly bind to pathogen-associated molecular patterns (PAMPs) and initiate immune responses that are collectively referred to as pattern-triggered immunity (PTI). Some of the PTI responses include changes in calcium (Ca^{2+}) levels, a burst in reactive oxygen species (ROS), mitogen-activated protein kinase (MPK) cascades, phytohormone signaling, and the induction of defense genes (*1*). Generally, PTI is sufficient to stave off nonadapted pathogens. However, adapted pathogens encode a suite of effectors that can suppress PTI. As a foil to pathogen effectors, plants have evolved intracellular nucleotide-binding leucine-rich repeat (NLR) class of immune receptors (*2*, *3*). NLRs contain coiled-coil (CC) or Toll/interleukin-1 receptor (TIR) homology domain at the N terminus and they are referred to as CNLs and TNLs, respectively. NLRs recognize pathogen effectors, either directly or indirectly, and trigger a substantially stronger immune response known as effector-triggered immunity (ETI) (*2*, *3*). ETI shares many of the same downstream responses as PTI; however, an ETI response often culminates in the hypersensitive response (HR), a form of programmed cell death (PCD) at the site of infection (HR-PCD) (*4*, *5*). HR-PCD is thought to effectively prevent pathogen spread from the infected cells to healthy cells. Recent evidence indicates that PTI can potentiate NLR-mediated, bacterial-derived ETI in Arabidopsis (*6*, *7*).

A growing body of evidence suggests that organelles such as chloroplasts play a central role in immunity (*8*–*11*). Chloroplasts are involved in the production of defense signaling molecules such as ROS and Ca^{2+} and also in the generation of precursors of defense hormones such as salicylic acid (SA), jasmonic acid, and abscisic acid (*12*, *13*). Chloroplasts have also been shown to function as defense-related motile organelles at fungal and oomycete pathogen entry sites (*14*, *15*).

There appears to be a direct communication between the plasma membrane and chloroplasts during immunity. PAMP perception at the plasma membrane not only induces rapid bursts of cytoplasmic Ca^{2+}, but also induces a long-lasting increase of Ca^{2+} concentration in the chloroplasts (*16*). The calcium-sensing receptor is a thylakoid-membrane localized protein that is required for chloroplast-Ca^{2+} concentration-dependent and PAMP-induced defense gene expression (*16*). Activation of PTI using effector deficient *Pseudomonas syringae* pv *tomato* (*Pst*) strain DC3000 also induces rapid production of ROS in the chloroplasts and changes in the expression levels of nuclear-encoded chloroplast genes (*17*). Perception of PAMPs has been shown to relocalize Arabidopsis calcium-dependent protein kinase 16 (CDPK16) from the plasma membrane to chloroplasts to induce defense responses (*18*). Chloroplasts also play a role in generating a sustained, second ROS burst during ETI (*19*). The ROS accumulation in chloroplasts during ETI is mediated by SA-induced protein kinase (SIPK) and wound-induced protein kinase (WIPK) in tobacco and their homologs MPK6 and MPK3 in Arabidopsis through the inhibition of photosynthesis (*19*, *20*).

Chloroplasts also play a direct role in NLR-mediated effector recognition and activation of ETI (*21*). Chloroplast-localized N receptor–interacting protein 1 (NRIP1) is required for tobacco N-TNL to recognize the p50 helicase domain of the tobacco mosaic virus (TMV) replicase (TMV-p50) and activate an immune response (*21*). NRIP1 relocalizes from chloroplasts to the cytoplasm and nucleus upon infection with TMV; this change in localization promotes N-TNL association with NRIP1 in the cytoplasm to recognize TMV-p50, activating ETI.

[1]Department of Plant Biology and The Genome Center, College of Biological Sciences, University of California, Davis, CA 95616, USA. [2]Department of Biological Sciences, College of Arts and Sciences, University of Delaware, Newark, DE 19716, USA. [3]Delaware Biotechnology Institute, University of Delaware, Newark, DE 19713, USA. [4]Department of Plant and Soil Sciences, College of Agriculture and Natural Resources, University of Delaware, Newark, DE 19716, USA.
*Corresponding author. Email: spdineshkumar@ucdavis.edu (S.P.D.-K.); jcaplan@udel.edu (J.L.C.)
†Present address: Carl Zeiss Microscopy, LLC, White Plains, NY 10601, USA.

Trafficking of the defense protein NRIP1 from chloroplasts to the nucleus during ETI is mediated by chloroplast stromules (*22*). Stromules are stroma-filled tubular extensions of the chloroplast envelope (*23*). Although stromules are present at a basal level in healthy tissue, they are significantly induced during PTI and ETI (*14*, *22*, *24*). Furthermore, exogenous application of defense signaling molecules, such as H_2O_2 and SA, is sufficient to induce stromule formation (*22*). Notably, stromules that are induced during ETI form complex associations with the nucleus and result in perinuclear chloroplast clustering (*21*, *25*). Our group and others have shown that stromules extend along microtubules (MTs) and that perturbations of the MT network disrupt stromule formation and stabilization of MTs induces stromules (*25*, *26*). Together, our previous work suggests that stromule extension along MTs, and subsequent anchoring to actin filaments (AFs) along nuclei, facilitates perinuclear chloroplast clustering during ETI (*25*). These

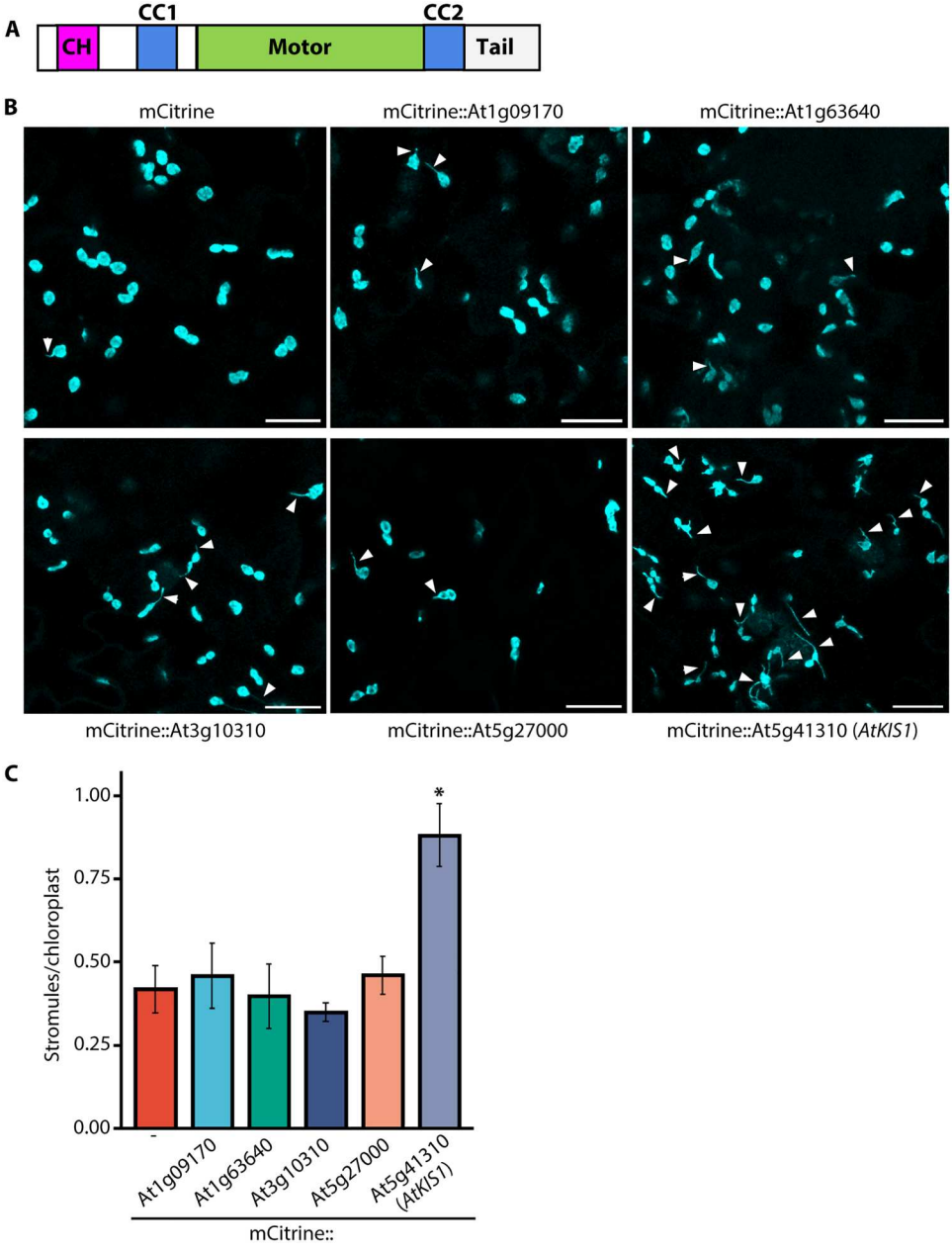

Fig. 1. Overexpression of an Arabidopsis kinesin with calponin homology domain, At5g41310, induces constitutive stromule formation. (**A**) Schematic diagram of a kinesin with CH domain at the N terminus, central motor domain flanked by CC domains, and C-terminal tail. (**B**) Representative confocal micrographs of stromule formation in epidermal cells of *Nicotiana benthamiana NN:NRIP1-Cerulean* plant leaves expressing mCitrine fused to different Arabidopsis CH domain–containing kinesins and mCitrine control. Images were collected 48 hours after infiltration. Arrows indicate stromules. Scale bar, 22 μm. (**C**) Quantification of stromule abundance from the experiment described in (B). Stromule abundance is defined as the number of stromules present in each image normalized by the number of chloroplasts. Data are represented as the means ± SEM, *$P < 0.05$, Student's *t* test ($n = 3$).

chloroplast-to-nucleus associations not only aid in the transport of NRIP1 but also in transporting chloroplast-produced hydrogen peroxide (H_2O_2) to the nucleus, potentially activating and/or reinforcing immunity (*22*). Perinuclear chloroplast clustering seems to be a general response to pathogen perception because it occurs during PTI and infection by viral and bacterial pathogens (*24*). Stromule formation is induced significantly at and around sites of HR-PCD, and this induction is SA-dependent (*22*, *27*). Constitutive induction of stromules can enhance NLR-mediated HR-PCD; suggesting that stromules have important functions during immunity (*22*). A recent report indicates that stromule induction is one of the earliest hallmarks of NLR-mediated immunity (*28*).

Although the findings over the past decade have shown that chloroplast stromules are induced during immunity and play a role in HR-PCD, the question of whether stromules are required for immunity still remains. To date, no genes or proteins have been identified which are required for stromule formation or function, presenting a major challenge in studying stromules' role. Here, we report the identification and characterization of a kinesin, containing an MT motor domain and an actin-binding calponin homology (CH) domain, which is required for stromule formation. We refer to this kinesin as kinesin required for inducing stromules 1 (KIS1). Knockdown of *KIS1* in *Nicotiana benthamiana* and knockout of *KIS1* in Arabidopsis abolish stromule formation during immunity. *KIS1* is required for NLR-mediated immunity against viral and bacterial pathogens. Overexpression of *KIS1* promotes constitutive stromule formation and perinuclear chloroplast clustering. Structure-function analysis indicates that stromule formation is a prerequisite for perinuclear chloroplast clustering, with perinuclear chloroplast clustering requiring an intact, actin-binding CH domain. *KIS1*-induced stromule formation requires early immune signaling components *ENHANCED DISEASE SUSCEPTIBILITY 1* (*EDS1*) and *PHYTOALEXIN DEFICIENT 4* (*PAD4*), while defense hormone SA-induced stromule formation requires *KIS1*.

RESULTS

Overexpression of a calponin homology domain containing kinesin, KIS1, induces stromules

Our previous report showed that chloroplast stromules use a cooperative action between MTs and AFs for locomotion throughout the cell (*25*). Therefore, we hypothesized that MTs act as tracks for stromule extension with AFs serving as anchor points to prevent stromule retraction back to the chloroplast body (*25*). Because of this observed cross-talk between MTs, AFs, and chloroplast stromules, we were specifically interested in proteins that may regulate stromule dynamics by interacting with both MTs and AFs. There is a plant-specific subfamily of kinesin-14s which contains a CH domain at the N terminus and a central MT-binding motor domain flanked by two CC domains (CC1 and CC2) (Fig. 1A) (*29*, *30*). Since CH domains are found in proteins known to bind AFs, kinesin with calponin homology domain (KCH) have been predicted to mediate cross-talk between MT and AF networks. Some plant KCHs have been shown to bind MTs and AFs (*31*–*36*). Therefore, we reasoned that KCH proteins could play a role in the cross-talk we observed between MTs, AFs, and chloroplast stromules during the immune response (*25*). To this end, we sought to determine whether the overexpression of one of the KCHs from *Arabidopsis thaliana* (Arabidopsis) could positively regulate stromule formation. We transiently expressed five of the six *At*KCHs under the control of the CaMV 35S promoter in transgenic *N. benthamiana* plants expressing the *N*-NLR immune receptor and chloroplast-localized NRIP1 fused to Cerulean fluorescent protein (*NN*::*NRIP1-Cerulean* plants hereafter) (*21*). NRIP1-Cerulean acts as a chloroplast stromal marker which facilitates monitoring of stromule induction and dynamics (*21*, *22*, *25*). We used our previously optimized methods to visualize and quantify stromules (*22*, *25*) (see Materials and Methods for details). Our results identified a single KCH, At5g41310, which induced a notable stromule phenotype, showing significant increases in the number of stromules formed in *NN*::*NRIP1-Cerulean* plant leaf epidermal cells (Fig. 1, B and C). In addition to the increase in stromule abundance, there was also significantly enhanced stromule dynamics (movie S1). We refer to At5g41310 as *At*KIS1. Notably, none of the other KCHs showed any significant change in stromule abundance compared to the monomeric citrine (mCitrine) control when overexpressed (Fig. 1, B and C). These results indicated that the stromule induction phenotype that we observed with *AtKIS1* is specific and not an artifact of overexpression.

KIS1 is required for stromule induction during NLR-mediated immunity

Previously, we have shown that stromules are significantly induced and play a role during bacterial and viral NLR immune receptor ETI (*22*). Since *AtKIS1* functions as a positive regulator of stromule formation (Fig. 1), we investigated whether *KIS1* is required for stromule induction during NLR-mediated ETI. For this, we decided to knock down the expression of *KIS1* in *N. benthamiana* using *Tobacco rattle virus* (TRV)–based virus-induced gene silencing (VIGS) (*37*). First, we identified the homolog of *AtKIS1* in *N. benthamiana* using the Sol Genomics Network database as Niben101Scf10389g01005.1 (*NbKIS1* hereafter). The amino acid sequence of *Nb*KIS1 is 50% identical and 70% similar to *At*KIS1 (figs. S1A and S2) and is phylogenetically closely related to *At*KIS1 (fig. S1B). Furthermore, *Nb*KIS1 contains a similar domain architecture to *At*KIS1; with an actin-binding CH domain, CC1, conserved neck motif, an MT-binding motor domain, a neck mimic motif, CC2, and a C terminus tail region (fig. S2). Then, we used this sequence to generate TRV-*NbKIS1* and knocked down the expression of *NbKIS1* (fig. S3) in *NN*::*NRIP1-Cerulean* plants, which exhibit stromule induction after delivering the TMV-p50 effector that is recognized by the N-NLR (*21*, *22*). Two weeks after TRV treatment, we expressed TMV-p50 effector via agro-infiltration in the TRV-*NbKIS1*–treated (referred to as *NbKIS1*-silenced) plants and TRV empty vector–treated (TRV-EV; nonsilenced) plants and measured stromule induction. As a positive control, we silenced the *N*-NLR immune receptor using TRV-*N* (*37*). Our results showed that TMV-p50 does not significantly induce stromule formation in *NbKIS1*-silenced *NN*::*NRIP1-Cerulean* plants compared to the transient expression of mCitrine (Fig. 2, A and B). As we have reported previously, silencing of *N*-NLR also compromises TMV-p50–induced stromule formation (Fig. 2, A and B). These results indicated that *NbKIS1* is required for stromule formation during the *N*-NLR–mediated immune response.

To further confirm the role of *KIS1* in stromule induction during immunity, we screened and identified two homozygous Arabidopsis T-DNA insertion mutants *Atkis1-1* and *Atkis1-2* (fig. S4, A to C).

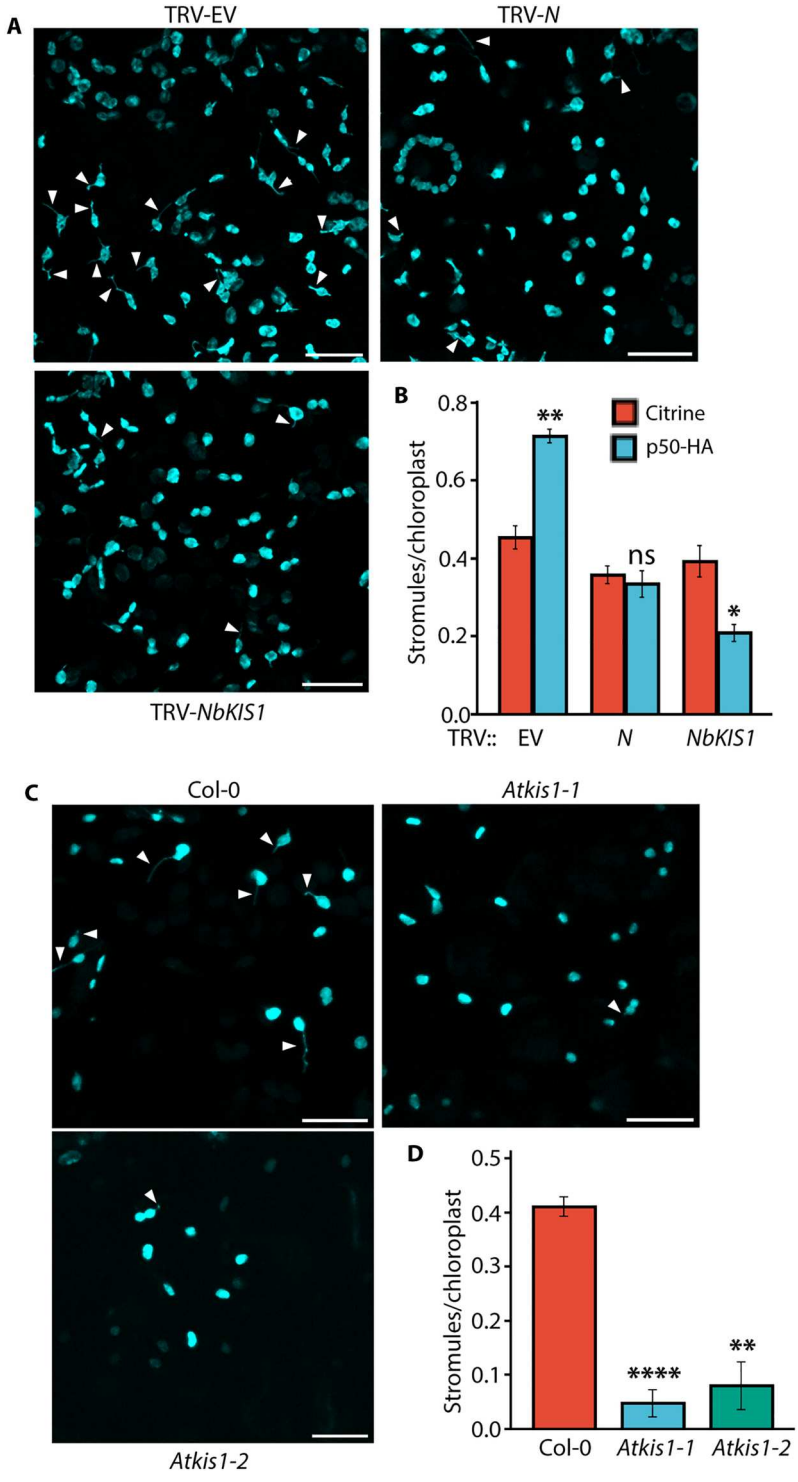

Fig. 2. KIS1 is required for stromule formation during the innate immune response. (**A**) Representative confocal micrographs of leaf epidermal cells of *NN:NRIP1-Cerulean* plants treated with *Tobacco rattle virus* empty vector as control (TRV-EV), TRV with *N* NLR (TRV-*N*), and TRV with *NbKIS1* (TRV-*NbKIS1*). Two weeks after silencing, leaves were Agro-infiltrated with TMV-p50-HA or citrine control, and images were collected 48 hours after infiltration. Arrows indicate stromules. Scale bars, 22 μm. (**B**) Quantification of stromule abundance for the experiment described in (A). Data are represented as the means ± SEM, $^{*}P < 0.05$ and $^{**}P < 0.01$, Student's *t* test ($n = 4$). (**C**) Representative confocal micrographs of leaf epidermal cells of wild type Col-0::NRIP1$_{cTP}$-tagCFP, *Atkis1-1*::NRIP1$_{cTP}$-tagCFP, and *Atkis1-2*::NRIP1$_{cTP}$-tagCFP plants 20 hours after infection with *Pst::AvrRPS4*. Arrows indicate stromules. Scale bars, 22 μm. (**D**) Quantification of stromule abundance from the experiment described in (C). Data are represented as the means ± SEM, $^{**}P < 0.01$ and $^{****}P < 0.0001$, Student's *t* test ($n = 8$). ns, not significant.

Reverse transcription polymerase chain reaction (RT-PCR) analysis showed that no *KIS1* transcripts were detectable in either mutant compared to the Col-0 control; hence, both *Atkis1-1* and *Atkis1-2* are null mutants (fig. S4D). Furthermore, *Atkis1* mutant plants have no apparent growth phenotype compared to the wild-type Col-0 plants (fig. S4E). To monitor stromule induction in *Atkis1* plants, we transformed both T-DNA insertion lines with a chloroplast stroma marker including chloroplast transit peptide of NRIP1 (NRIP1$_{cTP}$) fused to tagCFP (NRIP1$_{cTP}$-tCFP) under the control of ubiquitin promoter. Previously, we have shown that stromules are induced during the *RPS4*-NLR–mediated immune response to the *Pst* DC3000 strain expressing the *AvrRps4* effector (*Pst::AvrRps4*) in Arabidopsis (*22*). To test whether *AtKIS1* is required for stromule induction, we infiltrated *Pst::AvrRps4* into *Atkis1-1*::NRIP1$_{cTP}$-tCFP, *Atkis1-2*::NRIP1$_{cTP}$-tCFP, and control Col-0::NRIP1$_{cTP}$-tCFP plants. At 20 hours after infiltration with *Pst::AvrRps4*, we measured stromule induction. We observed significantly reduced stromule formation in both *Atkis1* mutants compared to Col-0 (Fig. 2, C and D). Together, these results indicated that *KIS1* is required for stromule formation and induction during NLR-mediated ETI.

KIS1-induced stromule formation is dependent on microtubules but not actin filaments

Since KIS1 contains both an actin-binding CH domain and an MT-binding motor domain, we determined the localization of KIS1 using AF and MT markers. We expressed 3xHA and monomeric Citrine fused to *AtKIS1* under the control of ubiquitin promoter (3xHA-mCitrine::*At*KIS1) with a previously described MT marker TagRFP-MAP-CKL6 (*25*) in *NN*::*NRIP1-Cerulean* plants. We observed a substantial overlap in localization between KIS1 and the MT marker (Fig. 3, A and B). KIS1 puncta were observed at stromule kinks and tips (Fig. 3, A and B). Colocalization with an actin marker, Lifeact-TagRFP, showed that KIS1 weakly localizes with the AFs (Fig. 3C) compared to the MTs (Fig. 3, A and B). KIS1 that colocalizes to the stromule kinks and tips does not colocalize with AF (Fig. 3C, arrows). Stromule tips without an accumulation of KIS1 were also observed (Fig 3A, asterisks).

Previously, we have shown that stromules extend along MTs and not AFs and that AFs have a separate function in stabilizing stromules (*25*). Therefore, we tested whether KIS1-induced stromule formation requires MTs or AFs. We expressed 3xHA-mCitrine::*At*KIS1 in *NN*::*NRIP1-Cerulean* plants and treated the leaves with oryzalin, to inhibit MTs, and cytochalasin D, to inhibit AFs, and measured stromule induction. Our results showed that, after oryzalin treatment, there was no significant increase in KIS1-induced stromules compared to mCitrine control (Fig. 3, D and E). However, both cytochalasin D and the mock buffer control treatment showed significant KIS1-induced stromule formation compared to mCitrine control (Fig. 3, D and E). These results indicate that KIS1-induced stromule formation only requires MTs.

CH domain of KIS1 is required for perinuclear chloroplast clustering

We and others have shown that the clustering of chloroplasts around the nucleus (perinuclear chloroplast clustering) is one of the hallmarks of the plant immune response (*24*, *25*). Furthermore, we have shown that chloroplasts move toward the nucleus through stromule-directed movement; with AFs playing an important role in mediating perinuclear chloroplast clustering during the immune response (*25*). Therefore, we tested if overexpression of KIS1 induces perinuclear chloroplast clustering and whether the actin-binding CH domain plays a role in this process. First, we assessed the role of different domains of KIS1 on KIS1-induced stromule formation. For this, we generated a number of in-frame deletion constructs with N-terminal 3xHA::mCitrine fusions (Fig. 4A). We confirmed the expression of the proteins from each of these deletion constructs through Agrobacterium-mediated transient expression in *NN*::*NRIP1-Cerulean* plants (fig. S5A). Deletion of the CH, CC1, and CC2 domains had no effect on KIS1-induced stromule formation (Fig. 4, A and B, and fig. S5B). In contrast, deletion of the motor domain and tail domain disrupted the robust stromule formation seen with full-length KIS1 (Fig. 4, A and B, and fig. S5B). Expression of the motor domain alone was not sufficient to induce stromule formation (Fig. 4, A and B, and fig. S5B). These results indicate that the actin-binding CH domain is not required for KIS1-induced stromule formation, while the MT-binding motor domain is required for KIS1-induced stromule induction. However, the motor domain alone is not sufficient to induce stromule formation. These results are consistent with the above-described MT and AF inhibitor experiments in which only the MT inhibitor affected KIS1-mediated stromule formation (Fig. 3, D and E).

Similar to what we have observed previously during the immune response (*25*), expression of KIS1 also promoted perinuclear chloroplast clustering compared to the mCitrine control (Fig. 4, C, panel 2 versus 1, and D, and movie S2). Since AFs are required for perinuclear chloroplast clustering (*25*), we tested whether deleting the CH domain, which can still induce stromule formation, is able to promote perinuclear chloroplast clustering. Our results showed that KIS1 without a CH domain does not induce perinuclear chloroplast clustering compared to the mCitrine control (Fig. 4, C, panel 2 versus 3, and D). The deletion of the CC1 and CC2 domains, which still exhibited KIS1-induced stromule formation (Fig. 4, A and B, and fig. S4B), also induced perinuclear chloroplast clustering (Fig. 4, C, panels 4 and 6, and D). In contrast, deletions of the motor and tail domain, which did not show KIS1-induced stromule formation, also did not induce significant perinuclear chloroplast clustering (Fig. 4, C, panels 5 and 7, and D). Consistent with this result, expression of the motor domain alone or motor domain with CC1 and CC2 also did not induce significant perinuclear chloroplast clustering (Fig. 4, C, panels 8 and 9, and D). These results indicate that stromule formation is a prerequisite to perinuclear chloroplast clustering and that an intact CH domain is required for KIS1-induced perinuclear chloroplast clustering.

KIS1 is required for *NLR*-mediated immunity

Since our findings show that *KIS1* is required for *NLR*-mediated stromule formation (Fig. 2), we tested whether *KIS1* is also required for cell death and immunity. For this, we silenced *NbKIS1* in *N. benthamiana* plants containing genomic *N*-NLR with exons and introns under its native promoter and 3′ end (*NN* plants) (*21*, *37*) as described above using TRV-VIGS. Two weeks after infiltration of the TRV-*NbKIS1* silencing construct, we conducted an ion leakage assay after infiltration with TMV-p50. Our results showed that the *NbKIS1*-silenced plants had ion leakage similar to that of TRV-*N*–treated plants and significantly less ion leakage compared to the TRV-EV control (Fig. 5A). These results indicated that *NbKIS1* is

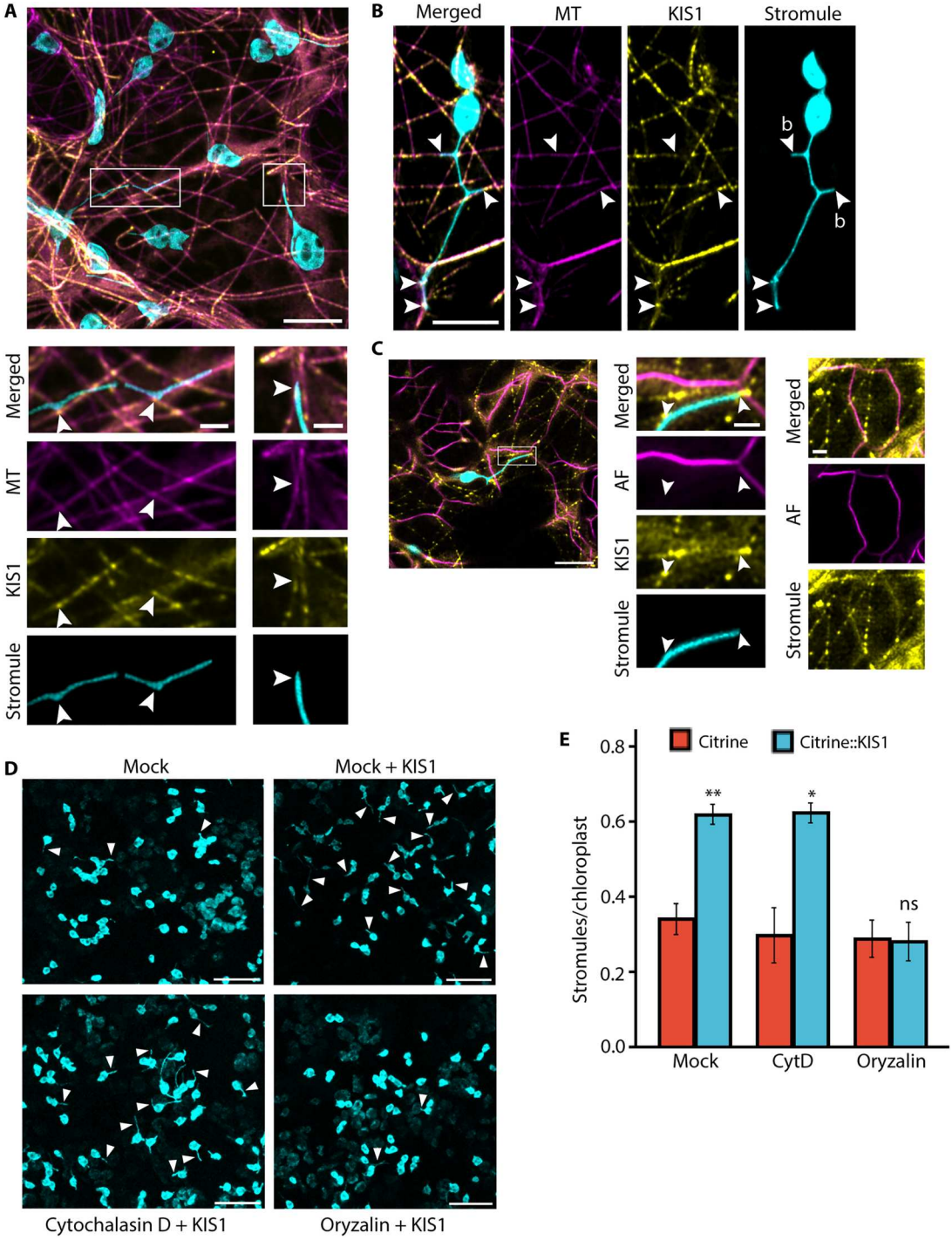

Fig. 3. KIS1 localizes to microtubules and is concentrated at stromule kinks and tips and microtubules are required for KIS1-induced stromule formation. (**A**) Citrine-KIS1 and the MT marker, TagRFP-MAP-CKL6, were transiently expressed in *NN:NRIP1-Cerulean* plants that mark stromules and then imaged by spinning disc confocal microscopy. Both stromules (cyan) and KIS1 (yellow) colocalized with MTs (magenta). Scale bar, 10 μm. Magnified views of the areas (white boxes) show examples of colocalization of KIS1 with stromule kinks (left, arrows) and a stromule tip (right, arrow). Scale bar, 2 μm. (**B**) Another representative example of KIS1 localized to a stromule kink and tip (arrow) and also colocalized with the tips of stromule branches (arrow, b). Scale bar, 10 μm. (**C**) Citrine-KIS1 and the actin marker, Lifeact-TagRFP, were transiently expressed in *NN:NRIP1-Cerulean* plants. The image shows stromule (cyan), KIS1 (yellow), and actin microfilament (magenta) localization. Scale bar, 10 μm (left). A magnified view of the area (white box) shows KIS1 localized to stromule kinks and tips did not colocalize with actin microfilaments (arrows). Scale bar, 2 μm (middle column). A detectable amount of KIS1 was found on actin microfilaments. Scale bar, 2 μm (right column). (**D**) Representative confocal micrographs of KIS1 overexpressing *NN:NRIP1-Cerulean* plants treated with AF and MT depolymerizing cytochalasin D (bottom left) and oryzalin (bottom right), respectively. The mock with mCitrine (top left) and the mock with KIS1 (top right) were used as controls. Arrows indicate stromules. Scale bars, 22 μm. (**E**) Quantification of the stromules from the experiment described in (D). Data are represented as the means ± SEM, $*P < 0.05$, $**P < 0.01$, Student's *t* test ($n = 4$).

required for immunity-induced cell death. To test whether *NbKIS1* is also required for immunity, we treated *NN* plants with the TRV-*NbKIS1*, TRV-*N*, and TRV-EV silencing constructs. We then sap-inoculated these silenced plants with equivalent titers of TMV. In resistant *NN* plants, TMV would be unable to spread past the inoculated leaves. In *NbKIS1*-silenced plants, TMV was able to move from the inoculated leaves into the upper parts of the plant resulting in tip death; unlike the control-silenced plants which showed no TMV movement or associated tip death (Fig. 5B). The loss-of-resistance phenotype observed in *NbKIS1*-silenced plants was similar to that of the *N*-NLR-silenced positive control plants (Fig. 5B). RT-PCR results confirmed the presence of TMV in the upper part of

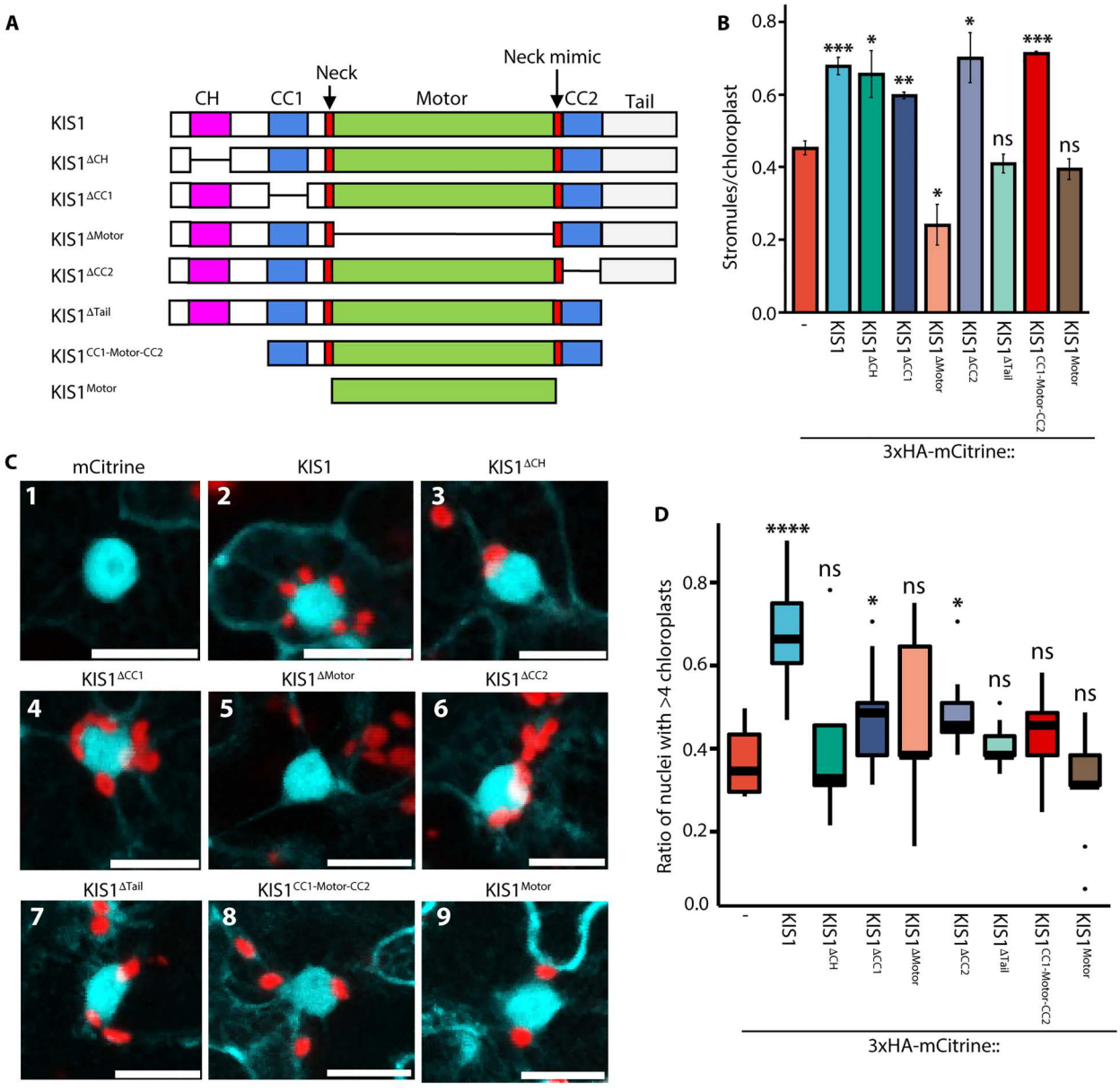

Fig. 4. The CH domain is required for KIS1-induced perinuclear chloroplast clustering. (**A**) Schematic diagram of full-length *At*KIS1 and different KIS1 domain deletions. CH, calponin homology domain; CC1, coiled-coil domain 1; Motor, kinesin motor domain; CC2, coiled-coil domain 2. (**B**) Quantification of stromule abundance from confocal micrographs (see fig. S4B) of plant leaves expressing AtKIS1 and different deletions shown in (A). Data are represented as the means ± SEM, $*P < 0.05$, $**P < 0.01$, and $***P < 0.001$, Student's *t* test ($n = 4$). (**C**) Representative confocal micrographs of perinuclear chloroplast clustering that is induced by overexpression of full-length KIS1 and different domain deletions in (A). Nuclei are marked by transiently expressing 35S:tagCFP and chloroplasts are marked by chlorophyll autofluorescence. Scale bars, 22 μm. (**D**) Quantification of perinuclear chloroplast clustering from the experiment described in (C). A nucleus was considered to be clustered if there were more than four chloroplasts directly in contact with the nucleus. Since nuclear clustering is a proportion, values were arcsine transformed before statistical testing. Boxes represent the second and third quartile range with whiskers being 1.5 times the interquartile range. $*P < 0.05$ and $****P < 0.0001$, Student's *t* test ($n = 9$).

the *NbKIS1*-silenced plants infected with TMV compared to the control-silenced plants (Fig. 5C). Together, these results indicate that *NbKIS1* plays a role in cell death and resistance to TMV.

We next used Arabidopsis *kis1* knockout mutants to further evaluate the role of *KIS1* in cell death and defense. Leaves of *Atkis1-1* and *Atkis1-2* knockout mutants were challenged with *Pst::AvrRps4*. After 20 hours, the leaves were stained with trypan blue to stain dead cells. We observed significantly less cell death in *Atkis1-1* and *Atkis1-2* knockout mutants compared to Col-0 wild-type plants (Fig. 5, D and E). Next, we assessed how this cell death affected bacterial growth. Our results showed that 3 days after infection, there is an increased amount of *Pst::AvrRps4* in both *Atkis1* knockout plants compared to the Col-0 control (Fig. 5F). Together, these results indicate that *KIS1* is required for the induction of cell death and resistance during ETI caused by bacterial and viral pathogens.

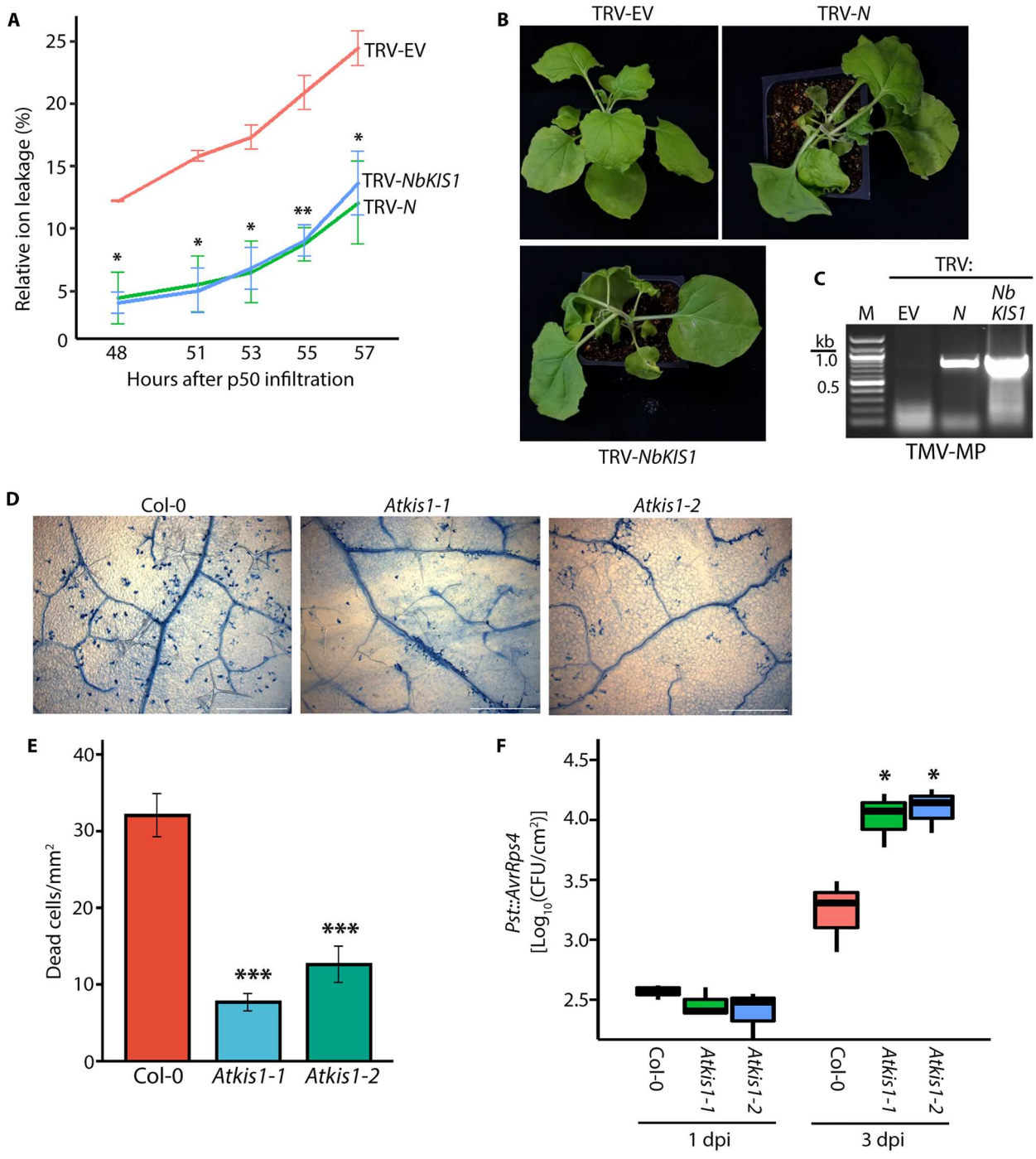

Fig. 5. KIS1 is required for *N* NLR- and *RPS4* NLR-mediated immunity. (**A**) Ion leakage analysis of *NN:NRIP1-Cerulean* plants treated with TRV-EV, TRV-*NbKIS1*, and TRV-*N* that were infiltrated with Agrobacterium-expressing TMV-p50 effector 2 weeks after silencing. Ion concentration was normalized by obtaining the maximum ion concentration for each replicate at the conclusion of the experiment. Data are represented as the means ± SEM, **P* < 0.05 and ***P* < 0.01, Student's *t* test (*n* = 3). (**B**) Representative photographs of *NN:NRIP1-Cerulean* plants treated with TRV-EV, TRV-*NbKIS1*, and TRV-*N* that were sap-inoculated with TMV 10 days after silencing. All of the *N*- and *NbKIS1*-silenced plants (three out of three) showed severe disease symptoms 10 days after infection with none of the TRV-EV control plants showing tip death characteristic of TMV spread. (**C**) RT-PCR analysis of TMV movement protein (TMV-MP) expression in the top leaves of the plants shown in (B). (**D**) Representative micrographs of trypan blue staining of Col-0 wild-type (WT) and *Atkis1-1* and *Atkis1-2* mutant plants 20 hours after infection by *Pst*::*AvrRPS4*. (**E**) Quantification of dead cells from the experiment described in (D). Data were normalized by the area of each micrograph. Data are represented as the means ± SEM, ****P* < 0.001, Student's *t* test (*n* = 6). (**F**) Quantification of bacterial titer at 1 and 3 days postinfection (dpi) by *Pst*::*AvrRPS4* in Col-0 WT and *Atkis1-1* and *Atkis1-2* mutant plants. Boxes represent the second and third quartile range with whiskers being 1.5 times the interquartile range. **P* < 0.05, Student's *t* test (*n* = 3).

KIS1-induced stromule formation is dependent on immune modulators *EDS1* and *PAD4*

Since our results show that KIS1 is an important player in stromule formation during immunity, we wanted to determine where in the immune signaling cascade KIS1 induces stromule formation. Most tested TNLs, including *N*, require the early signaling component *EDS1* which encodes a lipase-like protein (*37*–*39*). In addition, *N* and some TNLs require downstream CC helper NLR, *N REQUIREMENT GENE* 1 (*NRG1*) (*40*–*43*). In Arabidopsis, EDS1 complexes with PAD4 and functions through the ACTIVATED DISEASE RESISTANCE 1 (ADR1) helper NLR to promote transcriptional reprogramming and pathogen resistance (*44*–*46*). Before testing whether *EDS1*, *PAD4*, *NRG1*, and *ADR1* play a role in *KIS1*-induced stromule formation, we first determined if they are required for stromule induction during immunity. For this, we coexpressed genomic *N* with exons and introns under the control of the native promoter and 3′ end (p*N*::*N*) and TMV-p50-3xHA, which we have previously shown to induce cell death and defense (*21*, *47*), in *N. benthamiana eds1* (*Nbeds1*), *Nbpad4* (*48*), and *Nbnrg1* (*41*) knockout plants. Our results show that there was no significant increase in stromule formation with TMV-p50 treatment compared to the mCitrine control in either *Nbeds1*, *Nbpad4*, and *Nbnrg1* plants, unlike wild-type plants which showed robust stromule formation in response to TMV-p50 (Fig. 6, A and B). To test the role of *NbADR1* in stromule formation during immunity, we knocked down the expression of *NbADR1* using TRV-VIGS in *NN::NRIP1-Cerulean* plants (fig. S6) and expressed TMV-p50, similar to the previous experiments. Compared to TRV-EV–treated control plants, *NbADR1*-silenced plants did not show significant stromule formation, similar to the *N*-silenced positive control (Fig. 6, C and D). These results indicate that *NbEDS1*, *NbPAD4*, *NbNRG1*, and *NbADR1* are all required for stromule induction during *N* TNL–induced immune response.

Next, we wanted to determine whether *NbEDS1*, *NbPAD4*, *NbNRG1*, and *NbADR1* are required for *KIS1*-mediated stromule formation. We found that transient expression of *KIS1* was sufficient to induce stromule formation in *Nbnrg1* plants, but not in *Nbeds1* or *Nbpad4* knockout plants (Fig. 7, A and B). Furthermore, silencing of *NbADR1* had no effect on *KIS1*-induced stromule formation, with robust stromule formation 48 hours after KIS1 infiltration (Fig. 7, C and D). Together, these results indicate that only *NbEDS1* and *NbPAD4* are required for *KIS1*-induced stromule formation. These findings suggest that *KIS1* functions downstream of *EDS1* and *PAD4* but upstream of helper NLRs, *NRG1*, and *ADR1*.

SA-induced stromule formation requires *KIS1*

We reported that the exogenous application of the plant defense hormone, SA, is sufficient to induce stromule formation in the absence of pathogen infection (*22*). Since KIS1 is required for stromule induction and immunity, we wanted to determine whether we could rescue stromule formation in *NbKIS1*-silenced plants by exogenously applying SA in *NbKIS1* knockdown plants. For this, we infiltrated *NbKIS1*-silenced and TRV-EV control plants with 1 mM SA and measured stromule formation after 22 hours, as previously reported (*22*). Our results show that SA treatment does not induce stromule formation in *NbKIS1*-silenced plants compared to mock buffer infiltration, unlike the TRV-EV–treated plants which show robust stromule formation when treated with SA (Fig. 8A and fig. S7A). Next, we wanted to determine whether SA can induce stromule formation in *Nbeds1*, *Nbpad4*, and *Nbnrg1* knockouts, as well as in *NbADR1*-silenced plants. Our results show that exogenous application of SA fails to induce stromule formation in both *Nbeds1* and *Nbpad4* mutants compared to mock buffer control (Fig. 8, B and C, and fig. S7, B and C). In contrast, SA is sufficient to induce stromule formation in *Nbnrg1* plants as well as in *NbADR1*-silenced plants compared to the mock buffer control (Fig. 8, B and D, and fig. S7, B and D). Our quantitative RT-PCR (qRT-PCR) results showed that SA treatment has no effect on the expression of *KIS1* (fig. S8). Together, these results indicate that SA-induced stromule formation requires *KIS1*, *EDS1*, and *PAD4*.

DISCUSSION

Here, we have revealed a function for a KCH family kinesin, KIS1, in stromule formation and function during immunity. Previously, no genes known to function directly in stromule biogenesis had been identified. Although stromules were observed over a century ago (*49*–*52*), not until the advent of fluorescent protein markers combined with confocal microscopy and live cell imaging was their existence at basal levels in plant cells understood (*52*–*54*). However, until our report in 2015 (*22*), the biological function of stromules remained elusive. We demonstrated that stromules are induced during immunity and play a role in the transport of defense signals, such as H_2O_2 or the defense protein NRIP1, potentiating immunity-induced cell death (*22*). Since then, accumulating evidence indicates that the stromules are an integral part of a plant immune system (*14*, *15*, *24*–*28*). However, lacking genetic mutants with abolished stromule formation has severely hindered our ability to understand the direct role of stromules in immunity. Identification and characterization of KIS1 here have now provided direct evidence for stromules in immunity.

The kinesin-14 family, which includes KCHs, is unique to plants. However, the function of KCHs remains largely unknown. Rice OsKCH1 has been shown to regulate nuclear positioning (*55*) and Arabidopsis KinG has been shown to play a role in the intercellular movement of the SHORT-ROOT transcription factor in roots (*56*). In *Physcomitrella patens*, KCH has been shown to play a role in nuclear transport and tip growth of apical cells (*57*). Previously, there was no evidence linking a KCH to the plant immune response. Stromules are unable to form during the immune response in Arabidopsis *KIS1* knockouts and in *KIS1*-silenced *N. benthamiana* plants. We find that, in both *Atkis1* knockout plants and *NbKIS1*-silenced plants, stromules are still present at a basal level in the cell; however, they are not significantly induced in response to immune signals. It is possible that a subset of stromules does not require the cytoskeleton to form. Short stromules can be seen extending independently of the cytoskeleton and in isolated chloroplasts (*22*, *58*). In addition, our results show that loss of *KIS1* compromises *NLR*-mediated immunity to both viral and bacterial pathogens.

The KCH subfamily of kinesins is characteristic of containing a CH domain at the N terminus. In other organisms, CH domains are found in actin-binding proteins and play a role in actin dynamics and signaling (*31*, *32*, *59*). This characteristic makes KCH proteins unique, being MT-motor proteins that have actin-binding capabilities. Some plant KCHs have been shown to bind MT and AFs in vitro and in vivo (*33*, *34*, *60*–*62*). This characteristic cross-talk between AFs and MTs is what initially spurred our interest in the relationship between KCHs and stromule biogenesis. Our previous

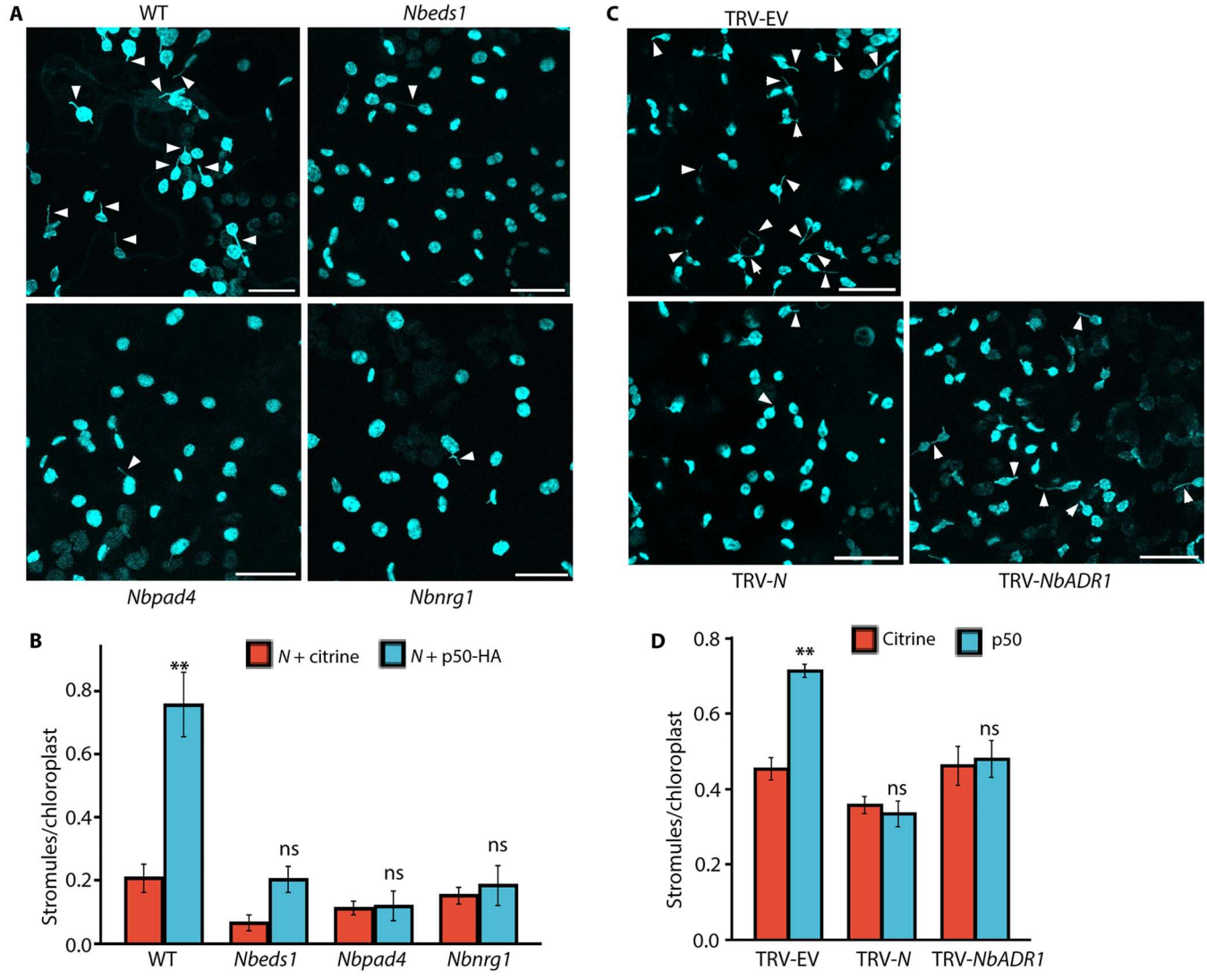

Fig. 6. Stromule induction during the *N* NLR-mediated immunity requires immune modulators *EDS1* and *PAD4* and helper NLRs, *NRG1*, and *ADR1*. (**A**) Representative confocal micrographs of leaf epidermal cells of WT, *Nbeds1*, *Nbpad4*, and *Nbnrg1* plants expressing *N* NLR with TMV-p50 effector or mCitrine control. To monitor stromule formation, chloroplast targeting peptide of AtRBCS1A fused to mNeonGreen under the control of 35S promoter (35S::AtRBCS1A$_{cTP}$-mNeonGreen) was expressed. Arrows indicate stromules. Scale bars, 22 μm. (**B**) Quantification of stromule formation from experiments described in (A). Data are represented as the means ± SEM, $^{**}P < 0.01$, Student's *t* test ($n = 4$). (**C**) Representative confocal micrographs of *NN:NRIP1-Cerulean* plants treated with TRV-EV, TRV-*N*, and TRV with *NbADR1* (TRV-*NbADR1*) that were infiltrated with TMV-p50 effector or mCitrine 2 weeks after silencing. Images were collected 48 hours after infiltration. Arrows indicate stromules. Scale bars, 22 μm. (**D**) Quantification of stromules from experiments described in (C). Data are represented as the means ± SEM, $^{**}P < 0.01$, Student's *t* test ($n = 4$).

findings showed that stromule dynamics require cross-talk between MTs and AFs (*25*). Our detailed structure-function analysis of KIS1 demonstrates that the actin-binding, CH domain is not required for stromule formation, whereas the MT-binding motor domain is required for stromule formation. Furthermore, disruption of MTs by oryzalin abolishes KIS1-induced stromule formation, while disruption of AFs, via cytochalasin D, has no effect on the KIS1-induced stromule formation. These results are consistent with our previous report that stromule formation requires MTs, while stromule anchoring and perinuclear chloroplast clustering require AFs (*25*). In line with these findings, our structure-function study also found that KIS1 does not require the actin-binding, CH domain to induce stromule formation; however, the stromules that form as a result are unable to induce perinuclear chloroplast clustering. These findings show that stromule formation alone is not sufficient to induce perinuclear chloroplast clustering. Since motor domain deletions of KIS1 abolish both stromule induction and perinuclear chloroplast clustering, stromule formation is therefore a prerequisite for inducing perinuclear chloroplast clustering.

Our findings using immune signaling mutants reveal that stromule induction is part of early immune signaling (Fig. 9). Our results using an *Nbeds1* mutant (*48*) indicate that the early immune signaling component *NbEDS1* is required for *N*-TNL–mediated stromule induction in response to TMV-p50. In addition, the

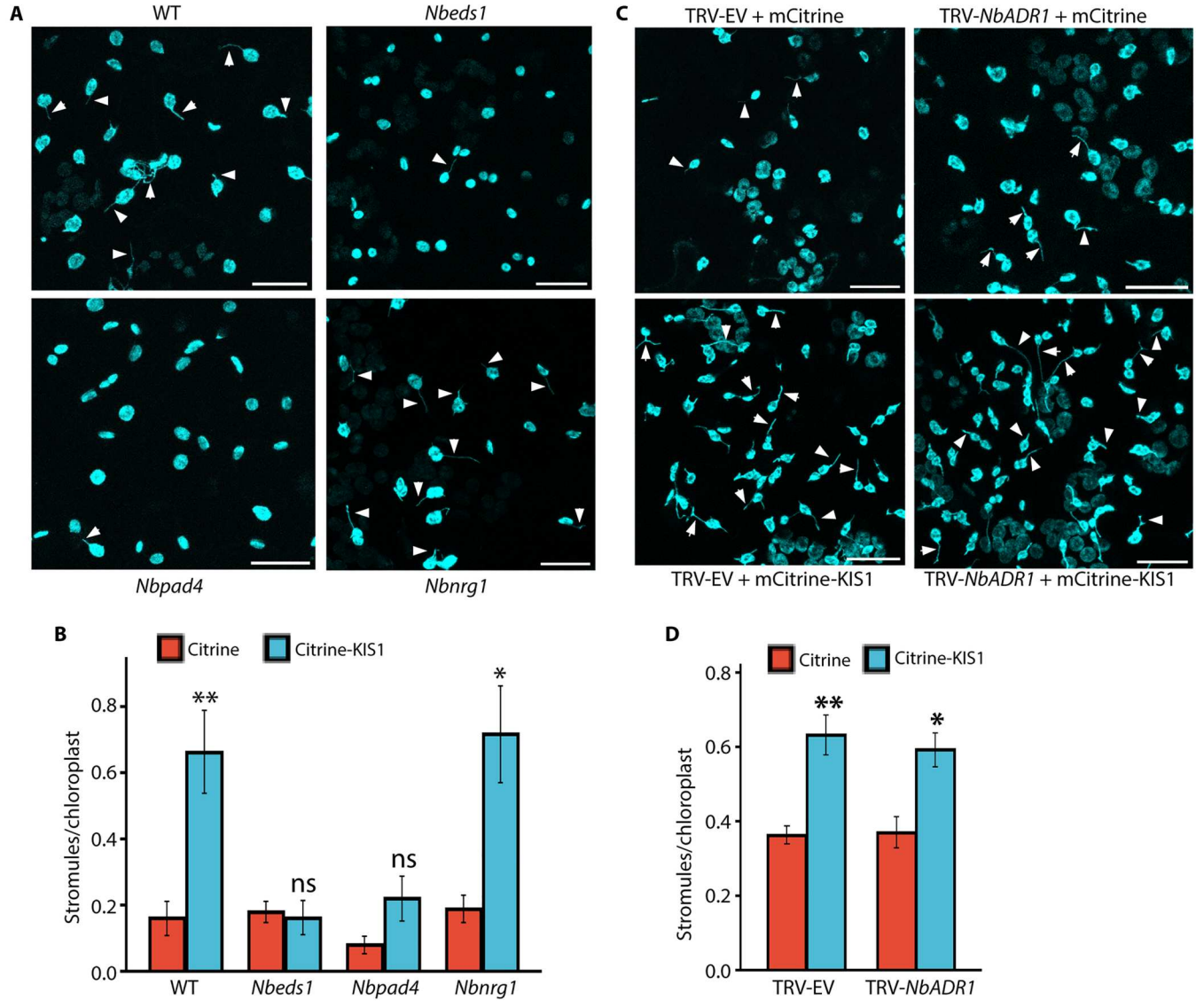

Fig. 7. KIS1-induced stromule formation is dependent on *EDS1* and *PAD4* and independent of *NRG1* and *ADR1*. (**A**) Representative confocal micrographs of leaf epidermal cells of WT, *Nbeds1*, *Nbpad4*, and *Nbnrg1* plants 48 hours after agro-infiltration of mCitrine-KIS1 or mCitrine control constructs. To monitor stromule formation, 35S::AtRBCS1A$_{CTP}$-mNeonGreen was expressed. Arrows indicate stromules. Scale bars, 22 μm. (**B**) Quantification of stromules from experiments described in (A). Data are represented as the means ± SEM, *P < 0.05 and **P < 0.01, Student's t test (n = 4). (**C**) Representative confocal micrographs of leaf epidermal cells of *NN:NRIP1-Cerulean* plants 10 days after treatment with TRV-EV and TRV-*NbADR1*. The micrographs are taken 48 hours after agro-infiltration with pUBQ::3xHA-mCitrine-KIS1 or mCitrine control constructs. Arrows indicate stromules. Scale bars, 22 μm. (**D**) Quantification of stromules from experiments described in (C). Data are represented as the means ± SEM, *P < 0.05 and **P < 0.01, Student's t test (n = 4).

helper NLR, *NbNRG1*, which functions with *EDS1* in inducing cell death is also required for *N*-TNL–induced stromule formation. EDS1 has been shown to associate with PAD4 to mediate transcriptional reprogramming of defense genes and pathogen resistance through the helper NLR, ADR1 (*44*–*46*). *N*-TNL–induced stromule formation also requires the function of *NbPAD4* and *NbADR1*. Collectively, our results reveal that an intact TNL immune signaling pathway is required for stromule induction in response to TMV-p50. Recently, Roq1-TNL–mediated stromule induction in response to XopQ effector from *Xanthomonas campestris* pv. *vesicatoria* has also been shown to require *NbEDS1*, *NbNRG1*, and *NbADR1* (*28*).

KIS1-induced stromule formation only requires *NbEDS1* and *NbPAD4* but not helper NLRs, *NbADR1*, and *NbNRG1* (Fig. 9). Recent structural studies indicated that the TIR domain of TNL generates small molecules such as 2-(5′-phosphoribosyl) adenosine 5′-monophosphate/diphosphate (pRib-AMP/ADP) and ADP-ribosylated adenosine 5′-triphosphate (ADPr-ATP) or ADP-ribosylated ADPR (di-ADPR) which bind to Arabidopsis EDS1-PAD4 and EDS1-SAG101 complexes, promoting their interaction with ADR1 and NRG1, respectively (*63*, *64*). Since only *NbEDS1* and *NbPAD4* are required for KIS1-induced stromule formation, it is possible that EDS1-PAD4 association with a helper NLR may not be required for KIS1-mediated stromule induction. Alternatively,

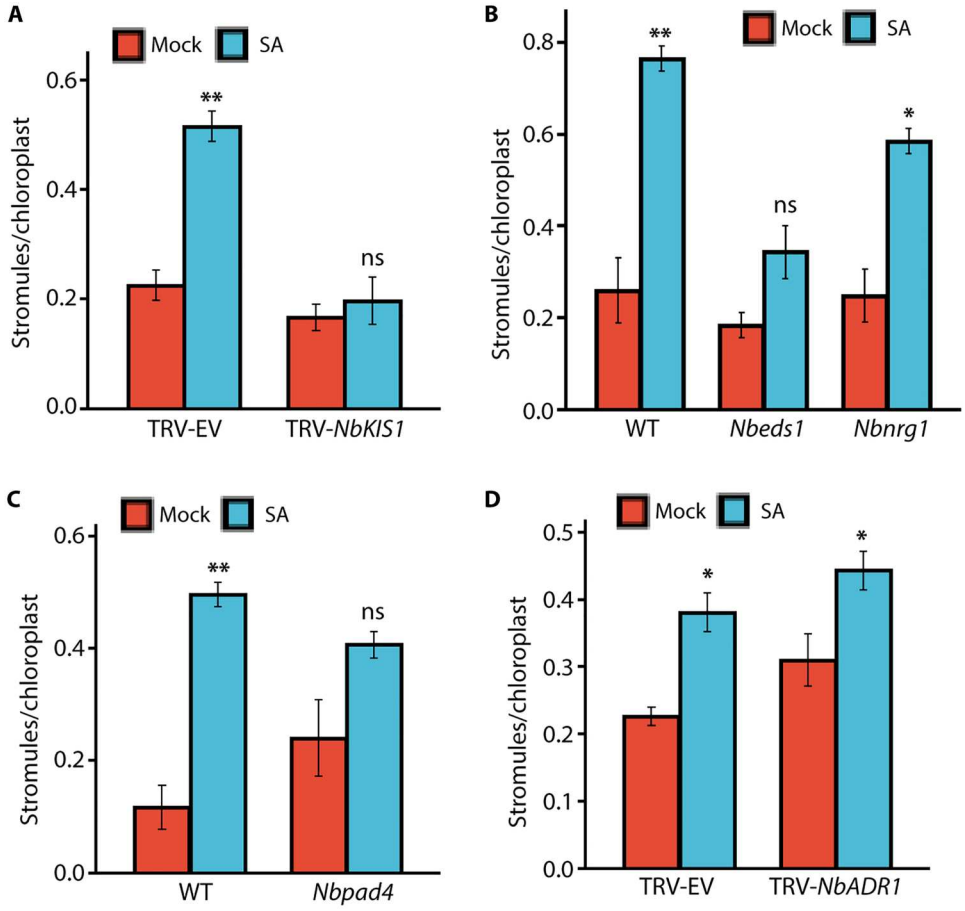

Fig. 8. KIS1 is required for salicylic acid–induced stromule formation. (**A**) Quantification of SA-induced stromule formation in *NN:NRIP1-Cerulean* plants treated with TRV-EV or TRV-*NbKIS1* using confocal micrographs from experiments described in fig. S7A. Data are represented as the means ± SEM, $^{**}P < 0.01$, Student's *t* test ($n = 3$). (**B**) Quantification of SA-induced stromule formation in WT and *Nbeds1* and *Nbnrg1* mutants using confocal micrographs from the experiment described in fig. S7B. Data are represented as the means ± SEM, $^{*}P < 0.05$, $^{**}P < 0.01$, Student's *t* test ($n = 3$). (**C**) Quantification of SA-induced stromule formation in WT and *Nbpad4* mutant using confocal micrographs from the experiment described in fig. S7C. Data are represented as the means ± SEM, $^{**}P < 0.01$, Student's *t* test ($n = 3$). (**D**) Quantification of SA-induced stromule formation in *NN:NRIP1-Cerulean* plants treated with TRV-EV or TRV-*NbKIS1* using confocal micrographs from experiments described in fig. S7D. Data are represented as the means ± SEM, $^{*}P < 0.05$, Student's *t* test ($n = 3$).

the nuclear function of EDS1 and PAD4 (*44*, *65*) may contribute to KIS1-induced stromule formation. A recent report showed that, in contrast to Arabidopsis, the binding of small molecules to EDS1 may not be required for TNL-mediated immunity; instead, nuclear EDS1 complexes are sufficient to induce ETI in *N. benthamiana* (*66*). Furthermore, the recent findings that the XopQ effector can induce stromule formation in *Nbnrg1* mutants support our findings that KIS1-induced stromule formation occurs upstream of *NbNRG1* but downstream of *NbEDS1* and *NbPAD4*.

Previously, we have shown that exogenous application of the defense hormone, SA, is sufficient to induce stromules (*22*). Our results described here show that KIS1 is required for SA-induced stromule formation. Similar to our findings with KIS1-induced stromule formation, SA-induced stromules also require *NbEDS1* and *NbPAD4*, but not *NbADR1* and *NbNRG1*. These results further point to the prominent role of *NbEDS1* and *NbPAD4* in stromule induction. Given that *EDS1* and *PAD4* play an important role in SA-mediated inhibition of pathogen growth, it will be interesting to further understand the role *EDS1* and *PAD4* play in KIS1- and SA-induced stromule formation during immunity.

In summary, we have identified a KCH, KIS1, which is required for stromule formation during the TNL-mediated immune response. Our data show that KIS1 is a key player in immunity. Considering that ETI-induced stromule formation is an integral part of immune response (*22*, *28*), future studies aimed at the identification of KIS1 interactors, and their function, should provide further insights into the role of KIS1 and stromules in immune signaling.

MATERIALS AND METHODS

Plant materials

Transgenic *N. benthamiana* with genomic *N*-NLR with exons and introns under its native promoter and 3′ end (*NN* plants) (*37*) and *NN*::*NRIP1-Cerulean* (*21*); CRISPR knockouts *Nbeds1* (*48*), *Nbnrg1* (*41*), and *Nbpad4* (*48*) lines have been described previously.

All Arabidopsis lines used in this study are in Columbia (Col-0) ecotype background. Arabidopsis T-DNA insertion lines

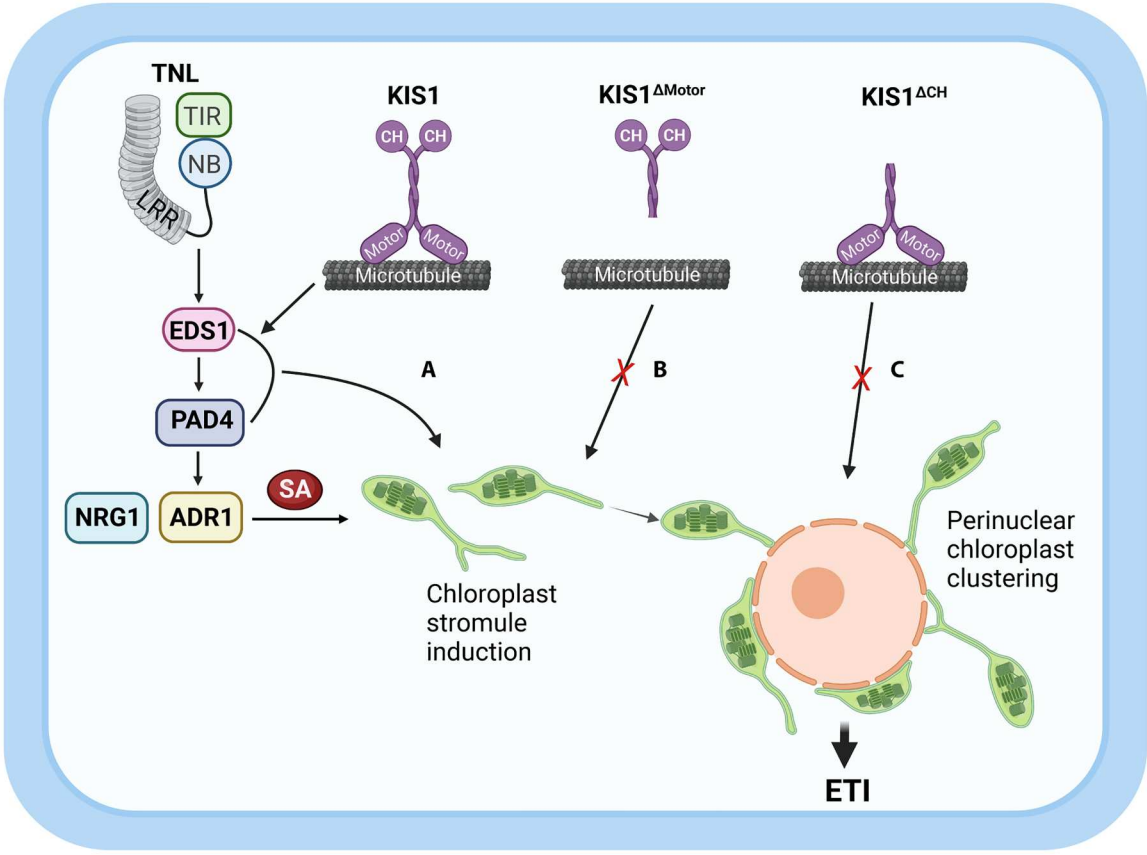

Fig. 9. The model shows KIS1 function in relation to known TNL-mediated immune signaling players to induce chloroplast stromule formation and perinuclear chloroplast clustering. While chloroplast stromules are a general byproduct of the TNL-mediated immune response, they require a fully intact TNL signaling pathway to be induced, including KIS1. Overexpression of KIS1 alone is sufficient to induce chloroplast stromule formation and subsequent perinuclear chloroplast clustering. Stromule formation induced by either KIS1 or SA is dependent on both EDS1 and PAD4 (a). Notably, KIS1-induced stromule formation requires a functional MT-binding motor domain (b). On the other hand, deletion of the actin-binding, CH domain in KIS1 leads to chloroplast stromule induction without subsequent perinuclear chloroplast clustering (c). Created with BioRender.com.

SALK_026963 (*Atkis1-1*) and SALK_117796 (*Atkis1-2*) were obtained from the Arabidopsis Biological Resource Center. T-DNA insertion lines were genotyped by PCR using gene-specific primers LP + RP and RP + LBb1.3 T-DNA–specific primer was listed in table S1.

Transgenic Arabidopsis plants were generated using the floral dip method (*67*). NRIP1$_{cTP}$-tCFP T-DNA plasmid was transformed into the GV3101 Agrobacterium strain and selected on LB agar plates with appropriate antibiotics. Agrobacterium harboring different constructs were grown overnight in 100 ml of LB liquid culture with appropriate antibiotics. Cells were pelleted and resuspended in a 5% (w/v) sucrose solution at an OD_{600} (optical density at 600 nm) = 0.8 with 0.05% Silwet L77. The above-ground parts of the flowering Col-0, *Atkis-1*, and *Atkis1-2* plants were dipped into the Agrobacterium solution for 10 s, with gentle agitation. After dipping, plants were wrapped in plastic film and stored in the dark at room temperature for 24 hours and moved to a controlled environment growth room. Seeds from dipped plants were harvested. Positive transformants were selected on ½ MS media containing BASTA (Glufosinate Ammonium) (7 μg/ml). T3 homozygous seeds of transgenic *Atkis1-1*::NRIP1$_{cTP}$-tCFP, *Atkis1-2*::NRIP1$_{cTP}$-tCFP, and Col-0::NRIP1$_{cTP}$-tCFP plants were used for the experiments.

Plant growth conditions

Wild-type *N. benthamiana*, various *Nb* mutants, and transgenic *NN*::*NRIP1-Cerulean* seeds were sown on Sunshine Mix 1 and were grown in a controlled environment chamber with 14-hour light and 10-hour dark photoperiod at 24°C.

Seeds of Arabidopsis Col-0, T-DNA insertion lines, and different transgenic lines were sown onto Sunshine Mix 1 soil and placed at 4°C for 5 days for stratification. Plants were grown in a controlled environment chamber under short-day conditions (8-hour light/16-hour dark) or long-day conditions at 22°C.

Plasmid construction

Plasmids TRV1(pYL192), TRV2-EV(pYL156), and TRV2-*N* (pYL155) (*37*), p*N*::*N*, TMV-p50-3xHA, mCitrine, tCFP (*21*, *47*), and TagRFP-MAP-CKL6 (SPDK2386) and Lifeact-TagRFP (SPDK2209) (*25*) have been described previously.

Different KCHs, At1g09170, At1g63640, At3g10310, At3g44730, At5g27000, and At5g41310 were PCR-amplified using primers listed in table S1 with Col-0 genomic DNA as template and cloned into *Avr*II-*Xma*I cut SPDK2734 T-DNA vector to generate p35S::mCitrine:*At*KCH:NOSterminator.

To generate TRV2-*NbKIS1* and TRV2-*NbADR1* vectors, PCR product was generated using primers listed in table S1 with *NbKIS1* cDNA and *N. benthamiana* genomic DNA as templates respectively were cloned into *Xba*I-*Sac*I cut pYL156(TRV2) (*37*).

To generate full-length *At*KIS1 fused to N-terminal 3xHA-mCitrine construct (NDM49), *At*KIS1 cDNA was cloned into a vector containing 3xHA-mCitrine under the control of ubiquitin promoter and nopaline synthase terminator. To generate the KIS1(-CH) construct (NDM51), two PCR products were generated using SP102964 + SP102695 and SP102696 + SP102697 primers with *At*KIS1 cDNA template, and the products were cloned into *Xma*I-*Mlu*I cut NDM49 using NEBuilder HiFi DNA Assembly Cloning Kit (New England Biolabs). Similarly, PCR products generated using primers SP102694 + SP102698 and SP102699 + SP102697; SP102694 + SP102700 and SP102701 + SP102697; SP102702 + SP102700 and SP102703 + SP102697; SP102694 + SP102704 and the resulting products were cloned into NDM49 using NEBuilder HiFi DNA Assembly Cloning Kit to generate KIS1(-CC1) (NDM52), KIS1(-Motor) (NDM53), KIS1(-CC2) (NDM54), and KIS1(-Tail) (NDM55) constructs, respectively. To generate the construct containing CC1-Motor-CC2 region of KIS1 (NDM56), PCR product was generated using SP102705 + SP102706 primers with *At*KIS1 cDNA template and cloned into NDM49 using NEBuilder HiFi DNA Assembly Cloning Kit. To generate the construct containing the motor domain of KIS1 alone (NDM57), PCR product was generated using SP102707 + SP102708 primers with AtKIS1 cDNA template and cloned into NDM49 using NEBuilder HiFi DNA Assembly Cloning Kit.

The stromule marker construct (SPDK3853: pUBQ::NRIP1$_{cTP}$-tCFP) was generated by cloning 330 base pairs of the genomic region of NRIP1 that include first intron into a vector containing tagCFP and 3xHA under the control of ubiquitin promoter and nopaline synthase terminator.

VIGS assay

NN::NRIP1-Cerulean or *NN* plants were used for the VIGS assay as described in (*21*, *37*). *Agrobacterium tumefaciens* GV2260 strain containing TRV1, TRV2-EV, TRV2-*N*, TRV2-*NbKIS1*, or TRV2-*NbADR1* were grown overnight, pelleted, resuspended in infiltration media (100 mM $MgCl_2$, 100 mM MES, and 250 μM acetosyringone) and brought to an OD_{600} = 0.5. Agrobacterium cultures were incubated at room temperature for 3 hours on a rotating slow shaker. TRV2-EV, TRV2-*N*, TRV2-*NbKIS1*, or TRV2-*NbADR1* was mixed with equal volumes of TRV1 and infiltrated into two opposite leaves of 10- to 14-day-old *NN* or *NN::NRIP1-Cerulean* plants. The infiltrated plants were left overnight in the laboratory and then transferred to the controlled environment chamber. For stromule observation, leaves of 10- to 14-day post-VIGS vector–treated plants were infiltrated with Agrobacterium containing p35S::TMV-p50-3xHA or p35S:mCitrine. Confocal microscopy was performed 48 hours after infiltration. After imaging, leaf tissue from the silenced plants was collected for qRT-PCR.

RNA isolation, RT-qPCR, and RT-PCR

To assess the silencing efficiency, RNA was extracted from leaves of plants treated with respective TRV-VIGS constructs using Direct-Zol RNA miniprep kit (Zymo Research). First-strand cDNA was generated from 1 μg of total RNA using the oligod(T) primer and OneScript Plus Reverse Transcriptase (Applied Biological Materials Inc). qPCR was performed using a Bio-Rad CFX96 Touch Real-Time PCR detection system (Bio-Rad) using iTaq universal SYBR Green Supermix (Bio-Rad). NbEF1α was used as an internal control to normalize the data. The fold change in mRNA levels was determined using the ΔΔCt method. For analysis of TMV infection, primer SP6289 that anneals to the 3′ end of movement protein (MP) gene of TMV was used to generate first-strand cDNA followed by PCR amplification of the MP region of TMV. As a control, first-strand cDNA was generated using oligod(T) primer followed by PCR amplification of NbeIF4a. Primers used for RT-qPCR and RT-PCR are listed in table S1.

TMV sap inoculation

Frozen *N. benthamiana* plant leaf tissue infected with TMV was ground using a pestle and mortar with freshly prepared, 100 mM sodium phosphate buffer, pH 7. The resulting emulsion was strained through a double-layered cheesecloth to remove leaf debris. The sap was then diluted with phosphate buffer to create an inoculum with a titer known to cause disease in wild-type *N. benthamiana* but not in p*N::N* transgenic *N. benthamiana* plants in our growth conditions. To inoculate plants, a small piece of cellulose sponge (HD Supply) was soaked in the inoculum, wrung out, and then rubbed onto three leaves per plant. Each silenced genotype was inoculated using a fresh sponge to avoid cross-contamination.

Ion leakage assay

The ion leakage experiments were conducted as described in (*68*). Briefly, 14 days after infiltration of TRV-*NbKIS1*, TRV-*N*, or TRV-EV into *NN* plants, the upper leaves were infiltrated with p35S::TMV-p50-3xHA. After 46 hours, two leaf discs were excised from the infiltrated leaf and used for the ion leakage assay. Measurements were taken every 2 hours for 12 hours using an electrolytic conductivity meter (HORIBA, model: B-173). After 12 hours, leaves were boiled in their respective wells and a final conductivity measurement was taken to determine relative ion leakage.

Trypan blue staining assay

Trypan blue staining was conducted as described in (*69*). Briefly, Arabidopsis plants were infiltrated with a syringe *Pst::AvrRps4* at an OD_{600} = 0.02. Twenty hours after infiltration, leaves for each tested genotype were collected and boiled in a trypan blue staining solution for 1 min. Samples were left at room temperature on a shaker for 24 hours. The trypan blue solution was removed and replaced with chloral hydrate destaining solution and allowed to shake for 6 hours at room temperature. The chloral hydrate solution was removed and replaced with fresh chloral hydrate solution and the samples were allowed to shake for another 12 hours at room temperature. Chloral hydrate solution was removed and replaced with 70% glycerol. Leaf samples were imaged with a Zeiss axioscan microscope.

Bacterial growth assay

The bacterial growth assay was conducted as described in (*70*). Briefly, 4- to 5-week-old Arabidopsis plants grown under short-day conditions were infiltrated with a syringe *Pst::AvrRps4* with an OD_{600} = 0.002. Plants were left covered with a plastic doom on the laboratory bench for 2 hours to allow leaves to dry. Following this, the plants were returned to the short-day growth conditions. The following day, one leaf disc from each infiltrated leaf was

collected and pooled. This was repeated three times for each genotype. The leaf discs were ground in 10 mM $MgCl_2$, and the resulting emulsion was serially diluted in 10 mM $MgCl_2$. Twenty milliliters of the serial dilution was plated onto King's B plates containing rifampicin (100 μg/ml) and kanamycin (25 μg/ml). The plates were incubated at 28°C for 2 days and bacterial colonies were counted and CFU-calculated as described in (*70*). This experiment was repeated independently three times with similar results.

Transient expression assay

A. tumefaciens GV3101 containing different expression vectors were grown overnight in LB media, pelleted, and resuspended in infiltration media (100 mM $MgCl_2$, 100 mM MES, and 250 μM Acetosyringone). *Agrobacterium* containing p35S::TMV-p50-3xHA or p35S:mCitrine was infiltrated into the leaf at an OD_{600} = 0.5. *Agrobacterium* containing full-length KCHs, full-length KIS1, and various KIS1 deletion constructs was infiltrated into the leaf at an OD_{600} = 1.0. For co-infiltration, *Agrobacterium* was mixed at equal volumes. All experiments were performed using 4- to 5-week-old *N. benthamiana* plants.

Laser scanning confocal microscopy

A Zeiss LSM 980 with an Airyscan 2 microscope with a Plan-apochromat 40× water immersion lens was used for live cell imaging. For imaging, 1-cm^2 leaf sections were excised from the infiltrated leaf area, distal to the syringe infiltration site. Images within the same figure were all captured using the same confocal settings and processed equally. The 445-, 488-, 514-, and 639-nm laser lines were used for Cerulean, mNeonGreen, mCitrine, and chlorophyll, respectively. For mCitrine-KIS1 localization, an Andor Dragonfly 600 spinning disc confocal on a Leica DMi8 microscope base was used for localization with the MT marker TagRFP-MAP-CKL6 and Lifeact-TagRFP in *NN::NRIP1-Cerulean* stromule marker line. A Leica HC Plan-apochromat 40×/1.1 NA water CS2 objective and the 445-, 515-, and 561-nm laser lines were used for Cerulean, mCitrine, and TagRFP, respectively.

Quantification of stromules

Stromules were quantified from *Z* stacks taken by confocal microscopy as described previously (*21*, *25*). Epidermal cells were imaged using 20- to 25-image *Z* stacks. Stromules were made visible by using chloroplast stroma-specific markers, which varied by experiment. The leaf area imaged for each dataset was kept consistent between treatments. Counting of stromules and chloroplasts was done by hand using Fiji (*71*). Stromule induction was quantified as the number of stromules normalized by the number of chloroplasts in any given image.

KIS1-induced and SA-induced stromule induction assay in *Nicotiana benthamiana* mutants and VIGS-silenced plants

Mutants, VIGS-silenced, and wild-type plants were syringe infiltrated with *Agrobacterium* containing p35S::AtRBCS1A$_{1-240bp}$::mNeonGreen. After this first infiltration, plants were left out overnight. The following day, either pUBQ::3xHA-mCitrine-*At*KIS1 at an OD_{600} = 1.0 or p35S:mCitrine at an OD_{600} = 1.0 was syringe-infiltrated into the same leaf as the mNeonGreen containing Agrobacterium; plants were then returned to their normal growth conditions. Confocal microscopy was performed 48 hours after the second infiltration as described earlier to monitor the stromule formation.

For SA-mediated stromule induction, mutants, VIGS-silenced, and wild-type plants were infiltrated with *Agrobacterium* containing p35S::AtRBCS1A$_{1-240bp}$::mNeonGreen. The following day, 1 mM SA in infiltration media or infiltration media alone was infiltrated into the same leaf as the *Agrobacterium*. Confocal microscopy was performed 22 hours after SA infiltration as described in (*22*) to monitor the stromule formation.

Western blot analysis

For Western blot, 100 mg of plant tissue expressing proteins of interest was collected and ground using a Mini-Beadbeater (Biospec Products). Two hundred microliters of 2× Laemmli sample buffer was added to the ground tissue and boiled for 5 min. The samples were briefly centrifuged, and the resulting supernatant was separated by SDS–polyacrylamide gel electrophoresis. Proteins were transferred to the Immobilon-P PVDF Membrane (Millipore, catalog number IPVH00010) using the Trans-Blot Turbo Transfer System (Bio-Rad). Membranes were blocked for 1 hour in 5% fat-free milk in phosphate-buffered saline with Tween 20 (PBST) and then incubated with rat anti-hemagglutinin antibody (1:5000 dilution; Roche, catalog number 11867423001) overnight at 4°C on a rocking platform. Blots were washed three times with PBST and incubated with anti-rat (1:5000 dilution; Santa Cruz Biotechnology, catalog number sc-2065) secondary antibody for 1 hour. Blots were washed three times with PBST and bands were visualized using SuperSignal West Pico PLUS Chemiluminescent Substrate (Thermo Fisher Scientific). Chemiluminescent signals were acquired using a ChemiDoc Touch Imaging System (Bio-Rad).

Cytoskeletal inhibitor assay

Actin inhibitor cytochalasin D and MT inhibitor oryzalin were prepared as 1 M stocks in dimethyl sulfoxide (DMSO). Before use, all the solutions were suspended in infiltration media at a working concentration. *N. benthamiana* leaves were infiltrated with pUBQ::3xHA-mCitrine-*At*KIS1 or p35S:mCitrine at 48 hours before imaging. One hour before imaging, treated leaves were infiltrated with 10 μM cytochalasin D, 1 μM oryzalin, or 0.1% DMSO in infiltration media. After one hour, a 1-cm^2 leaf distal to both infiltration sites was excised and mounted for imaging. Imaging and data analysis were performed as described above.

Perinuclear clustering assay

To visualize nuclei, wild-type *N. benthamiana* plants were co-infiltrated with *Agrobacterium* containing p35S::tagCFP along with either p35S:mCtrine, pUBQ:3xHA-mCitrine-*At*KIS1, or one of the AtKIS1 domain deletion constructs shown in Fig. 4A. After 48 hours, infiltrated leaves were imaged using a confocal microscope. Deep *Z* stacks were taken with a wide frame to capture as many nuclei per image as possible. Following confocal imaging, images were processed in Fiji (*71*). The number of nuclei marked by p35S::tagCFP and the number of chloroplasts, indicated by chlorophyll autofluorescence, were counted. In line with previous reports (*22*, *24*), a nucleus was considered clustered if there were >4 chloroplasts directly in contact with the nucleus.

Statistical analysis

In this study, graphs were all generated in R using the ggpubr (https://jtr13.github.io/cc20/brief-introduction-and-tutorial-of-ggpubr-package.html) package in R version 4.2.2 (R Core Team). For all comparative statistics, we used a Student's *t* test to determine the *P* value for the difference between means. Data from the perinuclear clustering experiment are a proportion and as such was arcsine transformed before performing any comparative statistics. For boxplots, boxes represent the second and third quartile range with whiskers being 1.5 times the interquartile range. For bar graphs, data are represented as the means ± SEM. $*P < 0.05$, $**P < 0.01$, $***P < 0.001$, and $****P < 0.0001$.

Supplementary Materials

This PDF file includes:

Figs. S1 to S8
Table S1
Legends for movies S1 and S2
Legend for full dataset Excel file
References

Other Supplementary Material for this manuscript includes the following:

Movies S1 and S2
Full dataset Excel file

REFERENCES AND NOTES

1. T. A. DeFalco, C. Zipfel, Molecular mechanisms of early plant pattern-triggered immune signaling. *Mol. Cell* **81**, 3449–3467 (2021).
2. J. D. G. Jones, J. L. Dangl, The plant immune system. *Nature* **444**, 323–329 (2006).
3. J. Wang, W. Song, J. Chai, Structure, biochemical function, and signaling mechanism of plant NLRs. *Mol. Plant* **16**, 75–95 (2023).
4. Y. Peng, R. van Wersch, Y. Zhang, Convergent and divergent signaling in PAMP-triggered immunity and effector-triggered immunity. *Mol. Plant Microbe Interact.* **31**, 403–409 (2018).
5. P. Balint-Kurti, The plant hypersensitive response: Concepts, control and consequences. *Mol. Plant Pathol.* **20**, 1163–1178 (2019).
6. M. Yuan, Z. Jiang, G. Bi, K. Nomura, M. Liu, Y. Wang, B. Cai, J. M. Zhou, S. Y. He, X. F. Xin, Pattern-recognition receptors are required for NLR-mediated plant immunity. *Nature* **592**, 105–109 (2021).
7. B. P. M. Ngou, H. K. Ahn, P. Ding, J. D. G. Jones, Mutual potentiation of plant immunity by cell-surface and intracellular receptors. *Nature* **592**, 110–115 (2021).
8. M. S. Padmanabhan, S. P. Dinesh-Kumar, All hands on deck—The role of chloroplasts, endoplasmic reticulum, and the nucleus in driving plant innate immunity. *Mol. Plant Microbe Interact.* **23**, 1368–1380 (2010).
9. E. Park, A. Nedo, J. L. Caplan, S. P. Dinesh-Kumar, Plant-microbe interactions: Organelles and the cytoskeleton in action. *New Phytol.* **217**, 1012–1028 (2018).
10. P. Kachroo, T. M. Burch-Smith, M. Grant, An emerging role for chloroplasts in disease and defense. *Annu. Rev. Phytopathol.* **59**, 423–445 (2021).
11. H. Irieda, Emerging roles of motile epidermal chloroplasts in plant immunity. *Int. J. Mol. Sci.* **23**, 4043 (2022).
12. E. Kuzniak, T. Kopczewski, The chloroplast reactive oxygen species-redox system in plant immunity and disease. *Front. Plant Sci.* **11**, 572686 (2020).
13. A. Bittner, A. Ciesla, K. Gruden, T. Lukan, S. Mahmud, M. Teige, U. C. Vothknecht, B. Wurzinger, Organelles and phytohormones: A network of interactions in plant stress responses. *J. Exp. Bot.* **73**, 7165–7181 (2022).
14. Z. Savage, C. Duggan, A. Toufexi, P. Pandey, Y. Liang, M. E. Segretin, L. H. Yuen, D. C. A. Gaboriau, A. Y. Leary, Y. Tumtas, V. Khandare, A. D. Ward, S. W. Botchway, B. C. Bateman, I. Pan, M. Schattat, I. Sparkes, T. O. Bozkurt, Chloroplasts alter their morphology and accumulate at the pathogen interface during infection by *Phytophthora infestans*. *Plant J.* **107**, 1771–1787 (2021).
15. H. Irieda, Y. Takano, Epidermal chloroplasts are defense-related motile organelles equipped with plant immune components. *Nat. Commun.* **12**, 2739 (2021).
16. H. Nomura, T. Komori, S. Uemura, Y. Kanda, K. Shimotani, K. Nakai, T. Furuichi, K. Takebayashi, T. Sugimoto, S. Sano, I. N. Suwastika, E. Fukusaki, H. Yoshioka, Y. Nakahira, T. Shiina, Chloroplast-mediated activation of plant immune signalling in Arabidopsis. *Nat. Commun.* **3**, 926 (2012).
17. M. Zabala, G. Littlejohn, S. Jayaraman, D. Studholme, T. Bailey, T. Lawson, M. Tillich, D. Licht, B. Bölter, L. Delfino, W. Truman, J. Mansfield, N. Smirnoff, M. Grant, Chloroplasts play a central role in plant defence and are targeted by pathogen effectors. *Nat. Plants* **1**, 1–10 (2015).
18. L. Medina-Puche, H. Tan, V. Dogra, M. Wu, T. Rosas-Diaz, L. Wang, X. Ding, D. Zhang, X. Fu, C. Kim, R. Lozano-Duran, A defense pathway linking plasma membrane and chloroplasts and co-opted by pathogens. *Cell* **182**, 1109–1124 (2020).
19. A. Shapiguzov, J. P. Vainonen, M. Wrzaczek, J. Kangasjarvi, ROS-talk - how the apoplast, the chloroplast, and the nucleus get the message through. *Front. Plant Sci.* **3**, 292 (2012).
20. J. Su, L. Yang, Q. Zhu, H. Wu, Y. He, Y. Liu, J. Xu, D. Jiang, S. Zhang, Active photosynthetic inhibition mediated by MPK3/MPK6 is critical to effector-triggered immunity. *PLOS Biol.* **16**, e2004122 (2018).
21. J. L. Caplan, P. Mamillapalli, T. M. Burch-Smith, K. Czymmek, S. P. Dinesh-Kumar, Chloroplastic protein NRIP1 mediates innate immune receptor recognition of a viral effector. *Cell* **132**, 449–462 (2008).
22. J. L. Caplan, A. S. Kumar, E. Park, M. S. Padmanabhan, K. Hoban, S. Modla, K. Czymmek, S. P. Dinesh-Kumar, Chloroplast stromules function during innate immunity. *Dev. Cell* **34**, 45–57 (2015).
23. M. R. Hanson, P. L. Conklin, Stromules, functional extensions of plastids within the plant cell. *Curr. Opin. Plant Biol.* **58**, 25–32 (2020).
24. X. Ding, T. Jimenez-Gongora, B. Krenz, R. Lozano-Duran, Chloroplast clustering around the nucleus is a general response to pathogen perception in *Nicotiana benthamiana*. *Mol. Plant Pathol.* **20**, 1298–1306 (2019).
25. A. S. Kumar, E. Park, A. Nedo, A. Alqarni, L. Ren, K. Hoban, S. Modla, J. H. McDonald, C. Kambhamettu, S. P. Dinesh-Kumar, J. L. Caplan, Stromule extension along microtubules coordinated with actin-mediated anchoring guides perinuclear chloroplast movement during innate immunity. *eLife* **7**, e23625 (2018).
26. J. L. Erickson, N. Adlung, C. Lampe, U. Bonas, M. H. Schattat, The *Xanthomonas* effector XopL uncovers the role of microtubules in stromule extension and dynamics in *Nicotiana benthamiana*. *Plant J.* **93**, 856–870 (2018).
27. T. Lukan, A. Zupanic, T. Mahkovec Povalej, J. O. Brunkard, M. Kmetic, M. Jutersek, S. Baebler, K. Gruden, Chloroplast redox state changes mark cell-to-cell signaling in the hypersensitive response. *New Phytol.* **237**, 548–562 (2023).
28. J. Prautsch, J. L. Erickson, S. Ozyurek, R. Gormanns, L. Franke, Y. Lu, J. Marx, F. Niemeyer, J. E. Parker, J. Stuttmann, M. H. Schattat, Effector XopQ-induced stromule formation in *Nicotiana benthamiana* depends on ETI signaling components ADR1 and NRG1. *Plant Physiol.* **191**, 161–176 (2023).
29. A. S. Reddy, I. S. Day, Kinesins in the Arabidopsis genome: A comparative analysis among eukaryotes. *BMC Genomics* **2**, 2 (2001).
30. Y.-R. J. Lee, B. Liu, Cytoskeletal motors in Arabidopsis. Sixty-one kinesins and seventeen myosins. *Plant Physiol.* **136**, 3877–3883 (2004).
31. M. Gimona, K. Djinovic-Carugo, W. J. Kranewitter, S. J. Winder, Functional plasticity of CH domains. *FEBS Lett.* **513**, 98–106 (2002).
32. E. Korenbaum, F. Rivero, Calponin homology domains at a glance. *J. Cell Sci.* **115**, 3543–3545 (2002).
33. M. L. Preuss, D. R. Kovar, Y. R. Lee, C. J. Staiger, D. P. Delmer, B. Liu, A plant-specific kinesin binds to actin microfilaments and interacts with cortical microtubules in cotton fibers. *Plant Physiol.* **136**, 3945–3955 (2004).
34. T. Xu, Z. Qu, X. Yang, X. Qin, J. Xiong, Y. Wang, D. Ren, G. Liu, A cotton kinesin GhKCH2 interacts with both microtubules and microfilaments. *Biochem. J.* **421**, 171–180 (2009).
35. N. Umezu, N. Umeki, T. Mitsui, K. Kondo, S. Maruta, Characterization of a novel rice kinesin O12 with a calponin homology domain. *J. Biochem.* **149**, 91–101 (2011).
36. J. Klotz, P. Nick, A novel actin-microtubule cross-linking kinesin, NtKCH, functions in cell expansion and division. *New Phytol.* **193**, 576–589 (2012).
37. Y. Liu, M. Schiff, R. Marathe, S. P. Dinesh-Kumar, Tobacco Rar1, EDS1 and NPR1/NIM1 like genes are required for *N*-mediated resistance to tobacco mosaic virus. *Plant J.* **30**, 415–429 (2002).
38. N. Aarts, M. Metz, E. Holub, B. J. Staskawicz, M. J. Daniels, J. E. Parker, Different requirements for EDS1 and NDR1 by disease resistance genes define at least two *R* gene-mediated signaling pathways in Arabidopsis. *Proc. Natl. Acad. Sci. U.S.A.* **95**, 10306–10311 (1998).
39. J. R. Peart, G. Cook, B. J. Feys, J. E. Parker, D. C. Baulcombe, An EDS1 orthologue is required for *N*-mediated resistance against tobacco mosaic virus. *Plant J.* **29**, 569–579 (2002).
40. J. R. Peart, P. Mestre, R. Lu, I. Malcuit, D. C. Baulcombe, NRG1, a CC-NB-LRR protein, together with N, a TIR-NB-LRR protein, mediates resistance against tobacco mosaic virus. *Curr. Biol.* **15**, 968–973 (2005).

41. T. Qi, K. Seong, D. P. T. Thomazella, J. R. Kim, J. Pham, E. Seo, M. J. Cho, A. Schultink, B. J. Staskawicz, NRG1 functions downstream of EDS1 to regulate TIR-NLR-mediated plant immunity in *Nicotiana benthamiana*. *Proc. Natl. Acad. Sci. U.S.A.* **115**, E10979–E10987 (2018).
42. B. Castel, P. M. Ngou, V. Cevik, A. Redkar, D. S. Kim, Y. Yang, P. Ding, J. D. G. Jones, Diverse NLR immune receptors activate defence via the RPW8-NLR NRG1. *New Phytol.* **222**, 966–980 (2019).
43. Z. Wu, M. Li, O. X. Dong, S. Xia, W. Liang, Y. Bao, G. Wasteneys, X. Li, Differential regulation of TNL-mediated immune signaling by redundant helper CNLs. *New Phytol.* **222**, 938–953 (2019).
44. H. Cui, E. Gobbato, B. Kracher, J. Qiu, J. Bautor, J. E. Parker, A core function of EDS1 with PAD4 is to protect the salicylic acid defense sector in Arabidopsis immunity. *New Phytol.* **213**, 1802–1817 (2017).
45. D. D. Bhandari, D. Lapin, B. Kracher, P. von Born, J. Bautor, K. Niefind, J. E. Parker, An EDS1 heterodimer signalling surface enforces timely reprogramming of immunity genes in *Arabidopsis*. *Nat. Commun.* **10**, 772 (2019).
46. X. Sun, D. Lapin, J. M. Feehan, S. C. Stolze, K. Kramer, J. A. Dongus, J. Rzemieniewski, S. Blanvillain-Baufume, A. Harzen, J. Bautor, P. Derbyshire, F. L. H. Menke, I. Finkemeier, H. Nakagami, J. D. G. Jones, J. E. Parker, Pathogen effector recognition-dependent association of NRG1 with EDS1 and SAG101 in TNL receptor immunity. *Nat. Commun.* **12**, 3335 (2021).
47. M. S. Padmanabhan, S. Ma, T. M. Burch-Smith, K. Czymmek, P. Huijser, S. P. Dinesh-Kumar, Novel positive regulatory role for the SPL6 transcription factor in the N TIR-NB-LRR receptor-mediated plant innate immunity. *PLOS Pathog.* **9**, e1003235 (2013).
48. J. Ordon, J. Gantner, J. Kemna, L. Schwalgun, M. Reschke, J. Streubel, J. Boch, J. Stuttmann, Generation of chromosomal deletions in dicotyledonous plants employing a user-friendly genome editing toolkit. *Plant J.* **89**, 155–168 (2017).
49. G. Haberlandt, Die Chlorophyllkrper der Selaginellen. *Flora* **71**, 291–308 (1988).
50. G. Senn, *Die Gestalts- und Lageverndерung der Pflanzen-Chromatophoren: mit einer Beilage: Die Lichtbrechung der lebenden Pflanzenzelle* (Wilhelm Engelmann Verlag, 1908).
51. K. Esau, Anatomical and cytological studies on beet mosaic. *J. Agric. Res.* **69**, 95–117 (1944).
52. J. C. Gray, J. A. Sullivan, J. M. Hibberd, M. R. Hanson, Stromules: Mobile protrusions and interconnections between plastids. *Plant Biol.* **3**, 223–233 (2001).
53. D. Menzel, An interconnected plastidom in *Acetabularia*: Implications for the mechanism of chloroplast motility. *Protoplasma* **179**, 166–171 (1994).
54. R. H. Kohler, J. Cao, W. R. Zipfel, W. W. Webb, M. R. Hanson, Exchange of protein molecules through connections between higher plant plastids. *Science* **276**, 2039–2042 (1997).
55. N. Frey, J. Klotz, P. Nick, A kinesin with calponin-homology domain is involved in premitotic nuclear migration. *J. Exp. Bot.* **61**, 3423–3437 (2010).
56. Z. Spiegelman, C. M. Lee, K. L. Gallagher, KinG is a plant-specific kinesin that regulates both intra- and intercellular movement of SHORT-ROOT. *Plant Physiol.* **176**, 392–405 (2018).
57. M. Yamada, G. Goshima, The KCH kinesin drives nuclear transport and cytoskeletal coalescence to promote tip cell growth in *Physcomitrella patens*. *Plant Cell* **30**, 1496–1510 (2018).
58. J. O. Brunkard, A. M. Runkel, P. C. Zambryski, Chloroplasts extend stromules independently and in response to internal redox signals. *Proc. Natl. Acad. Sci. U.S.A.* **112**, 10044–10049 (2015).
59. L. M. Yin, M. Schnoor, C.-D. Jun, Structural characteristics, binding partners and related diseases of the calponin homology (CH) domain. *Front. Cell Dev. Biol.* **8**, 342 (2020).
60. N. Frey, J. Klotz, P. Nick, Dynamic bridges—A calponin-domain kinesin from rice links actin filaments and microtubules in both cycling and non-cycling cells. *Plant Cell Physiol.* **50**, 1493–1506 (2009).
61. W. J. Walter, I. Machens, F. Rafieian, S. Diez, The non-processive rice kinesin-14 OsKCH1 transports actin filaments along microtubules with two distinct velocities. *Nat. Plants* **1**, 15111 (2015).
62. K. F. Tseng, P. Wang, Y. J. Lee, J. Bowen, A. M. Gicking, L. Guo, B. Liu, W. Qiu, The preprophase band-associated kinesin-14 OsKCH2 is a processive minus-end-directed microtubule motor. *Nat. Commun.* **9**, 1067 (2018).
63. S. Huang, A. Jia, W. Song, G. Hessler, Y. Meng, Y. Sun, L. Xu, H. Laessle, J. Jirschitzka, S. Ma, Y. Xiao, D. Yu, J. Hou, R. Liu, H. Sun, X. Liu, Z. Han, J. Chang, J. E. Parker, J. Chai, Identification and receptor mechanism of TIR-catalyzed small molecules in plant immunity. *Science* **377**, eabq3297 (2022).
64. A. Jia, S. Huang, W. Song, J. Wang, Y. Meng, Y. Sun, L. Xu, H. Laessle, J. Jirschitzka, J. Hou, T. Zhang, W. Yu, G. Hessler, E. Li, S. Ma, D. Yu, J. Gebauer, U. Baumann, X. Liu, Z. Han, J. Chang, J. E. Parker, J. Chai, TIR-catalyzed ADP-ribosylation reactions produce signaling molecules for plant immunity. *Science* **377**, eabq8180 (2022).
65. A. V. Garcia, S. Blanvillain-Baufume, R. P. Huibers, M. Wiermer, G. Li, E. Gobbato, S. Rietz, J. E. Parker, Balanced nuclear and cytoplasmic activities of EDS1 are required for a complete plant innate immune response. *PLOS Pathog.* **6**, e1000970 (2010).
66. J. Zonnchen, J. Gantner, D. Lapin, K. Barthel, L. Eschen-Lippold, J. L. Erickson, S. L. Villanueva, S. Zantop, C. Kretschmer, M. Joosten, J. E. Parker, R. Guerois, J. Stuttmann, EDS1 complexes are not required for PRR responses and execute TNL-ETI from the nucleus in *Nicotiana benthamiana*. *New Phytol.* **236**, 2249–2264 (2022).
67. S. J. Clough, A. F. Bent, Floral dip: A simplified method for Agrobacterium-mediated transformation of *Arabidopsis thaliana*. *Plant J.* **16**, 735–743 (1998).
68. N. Hatsugai, F. Katagiri, Quantification of plant cell death by electrolyte leakage assay. *Bio. Protoc.* **8**, e2758 (2018).
69. S. van Wees, *Phenotypic Analysis of Arabidopsis Mutants: Trypan Blue Stain for Fungi, Oomycetes, and Dead Plant Cells* (Cold Spring Harbor Laboratory Press, 2008).
70. X. Liu, Y. Sun, C. J. Korner, X. Du, M. E. Vollmer, K. M. Pajerowska-Mukhtar, Bacterial leaf infiltration assay for fine characterization of plant defense responses using the *Arabidopsis thaliana-Pseudomonas syringae* pathosystem. *J. Vis. Exp.*, 53364 (2015).
71. J. Schindelin, I. Arganda-Carreras, E. Frise, V. Kaynig, M. Longair, T. Pietzsch, S. Preibisch, C. Rueden, S. Saalfeld, B. Schmid, J. Y. Tinevez, D. J. White, V. Hartenstein, K. Eliceiri, P. Tomancak, A. Cardona, Fiji: An open-source platform for biological-image analysis. *Nat. Methods* **9**, 676–682 (2012).
72. D. T. Jones, W. R. Taylor, J. M. Thornton, The rapid generation of mutation data matrices from protein sequences. *Comput. Appl. Biosci.* **8**, 275–282 (1992).
73. K. Tamura, G. Stecher, S. Kumar, MEGA11: Molecular evolutionary genetics analysis version 11. *Mol. Biol. Evol.* **38**, 3022–3027 (2021).

Acknowledgments: We thank J. Stuttmann and J. Parker for *Nbeds1* and *NbPad4* seeds and B. Staskawicz for *Nbnrg1* seeds. **Funding:** This work was supported by NIH grant R01GM132582 to S.P.D.-K. and J.L.C. and USDA National Institute of Food and Agriculture (USDA-NIFA) predoctoral fellowship grant 2021-67034-35187 to N.D.M. Microscopes used for the work performed for this paper were supported by NIH grants S10OD026702, S10OD030321, and P20 GM103446. **Author contributions:** Conceptualization: N.D.M., J.L.C., and S.P.D.-K. Methodology and analyses: N.D.M., K.S., J.L.C., and S.P.D.-K. Writing—original draft: N.D.M., J.L.C., and S.P.D.-K. Writing—reviewing and editing: N.D.M., K.S., J.L.C., and S.P.D.-K. **Competing interests:** The authors declare that they have no competing interests. **Data and materials availability:** All data needed to evaluate the conclusions of the paper are present in the paper and/or the Supplementary Materials.

Submitted 15 May 2023
Accepted 25 September 2023
Published 25 October 2023
10.1126/sciadv.adi7407